







Developmental origins of Parkinson's disease risk: perinatal exposure to the organochlorine pesticide dieldrin leads to sex-specific DNA modifications in critical neurodevelopmental pathways in the mouse midbrain

Joseph Kochmanski ¹, Mahek Virani ², Nathan C. Kuhn¹, Sierra L. Boyd ¹, Katelyn Becker ³, Marie Adams ³, Alison I. Bernstein ^{1,2,4,*}

¹Department of Translational Neuroscience, College of Human Medicine, Michigan State University, Grand Rapids, MI 49503, United States

²Department of Pharmacology and Toxicology, Ernest Mario School of Pharmacy, Rutgers University, Piscataway, NJ 08854, United States

³Genomics Core, Van Andel Research Institute, Grand Rapids, MI 49503, United States

⁴Environmental and Occupational Health Sciences Institute, Ernest Mario School of Pharmacy, Rutgers University, Piscataway, NJ 08854, United States

*Corresponding author: Environmental and Occupational Health Sciences Institute, Ernest Mario School of Pharmacy, Rutgers University, 170, Freylinghuysen Road, Piscataway, NJ 08854, United States. Email: bernstein.alison@rutgers.edu

Abstract

Epidemiological studies show that exposure to the organochlorine pesticide dieldrin is associated with an increased risk of Parkinson's disease (PD). Animal studies support a link between developmental dieldrin exposure and increased neuronal susceptibility in the α -synuclein preformed fibril and MPTP models in adult male C57BL/6 mice. In a previous study, we showed that developmental dieldrin exposure was associated with sex-specific changes in DNA modifications within genes related to dopaminergic neuron development and maintenance at 12 wk of age. Here, we used capture hybridization-sequencing with custom baits to interrogate DNA modifications across the entire genetic loci of the previously identified genes at multiple time points—birth, 6, 12, and 36 wk old. We identified largely sex-specific dieldrin-induced changes in DNA modifications at each time point that annotated to pathways important for neurodevelopment, potentially related to critical steps in early neurodevelopment, dopaminergic neuron differentiation, synaptogenesis, synaptic plasticity, and glial-neuron interactions. Despite large numbers of age-specific DNA modifications, longitudinal analysis identified a small number of differential modification of cytosines with dieldrin-induced deflection of epigenetic aging. The sex-specificity of these results adds to evidence that sex-specific responses to PD-related exposures may underly sex-specific differences in disease. Overall, these data support the idea that developmental dieldrin exposure leads to changes in epigenetic patterns that persist after the exposure period and disrupt critical neurodevelopmental pathways, thereby impacting risk of late-life diseases, including PD.

Keywords: dieldrin; pesticides; DNA methylation; epigenetics; Parkinson's disease

Parkinson's disease (PD) is the most common neurodegenerative movement disorder and one of the fastest-growing neurological diseases worldwide (Dorsey et al. 2007, 2018a, 2018b; Marras et al. 2018; Yang et al. 2020; Willis et al. 2022). PD diagnoses in the US cluster in regions with a history of industrialization—e.g. the Midwest and Northeast—and worldwide rates of disease are increasing most rapidly in newly industrialized regions, suggesting that environmental factors related to industrialization play an important role in PD etiology (Dorsey et al. 2007; Willis et al. 2010; Willis et al. 2022). In addition, multiple animal studies have shown that exposure to specific environmental toxicants, including certain industrial toxicants, heavy metals, and pesticides, is associated with an increased risk of PD (Cicchetti et al. 2009; Moretto and Colosio 2011; Caudle et al. 2012; Freire and Koifman 2012; Goldman 2014; Goldman et al. 2017).

Further supporting the idea that environment plays a role in PD etiology, the vast majority (90% to 95%) of PD cases are sporadic, with monogenic mutations responsible for only 5% to 10% of PD cases (Trinh and Farrer 2013; Lill 2016). In addition, heritability estimates suggest that only about a third of the phenotypic variance of sporadic PD can be explained by genetics (Keller et al. 2012; Fernández-Santiago and Sharma 2022). Thus, the etiology of sporadic PD is thought to involve complex interactions between aging, genetics, and environmental risk factors (Cannon and Greenamyre 2013; Fleming 2017; Bogers et al. 2023). The epigenome is recognized as a potential mediator of this relationship due to its unique sensitivity to the environment, establishment during cellular differentiation, and potential to regulate gene expression throughout the lifespan (Faulk and Dolinoy 2011; Allis and Jenuwein 2016; Bianco-Miotto et al. 2017). Given these

characteristics, it is hypothesized that developmental exposures induce fixed changes in the epigenome, creating a poised epigenetic state in which exposure programs a modified response to later-life challenges resulting in altered disease risk (Svoboda et al. 2022b). A growing body of work suggests that the epigenetic mechanisms serve as a mediator of environmental risk factors in PD (Schaffner and Kobor 2022; Tsalenchuk et al. 2023; Gionco and Bernstein 2024).

According to the developmental origins of health and disease (DoHAD) hypothesis, exposures, even during prenatal development, can produce long-lasting changes in gene regulation and neurodevelopment that contribute to the risk of later-life disease (Hochberg et al. 2011; Heindel and Vandenberg 2015). In such a model, the toxicant-induced mechanisms that contribute to PD risk may be temporally separated from disease onset and represent early predegenerative changes. Two-hit models of PD, including the developmental dieldrin α -synuclein preformed fibril (α -syn PFF) model developed in our lab, offer an opportunity to explore the effects of environmental exposures and to identify predegenerative changes that occur prior to the onset of neurodegeneration and set the stage for increased susceptibility to disease (Richardson et al. 2006; Gezer et al. 2020; Boyd et al. 2023). Using two-hit models, work from our lab and others has established the developmental dieldrin exposure model as a model of increased PD susceptibility (Richardson et al. 2006; Kochmanski et al. 2019; Gezer et al. 2020; Boyd et al. 2023).

Dieldrin is an organochlorine pesticide that was phased out of commercial use due to toxicological concerns in the 1970s, but the chemical persists in the environment and lipid-rich tissues like the brain due to its high stability and lipophilicity (Jorgenson 2001; Agency for Toxic Substances and Disease Registry 2022). Mechanistic animal studies demonstrate that adult and developmental dieldrin exposures are associated with disrupted expression of PD-related proteins, oxidative stress, and increased susceptibility to secondary toxicants that affect the dopaminergic system (Richardson et al. 2006; Hatcher et al. 2007; Kochmanski et al. 2019; Gezer et al. 2020; Boyd et al. 2023). Specifically, adult male C57BL/6 mice developmentally exposed to dieldrin show exacerbated neurotoxicity in adulthood (12 wk of age) induced by synucleinopathy in the α -syn PFF model and by MPTP (Richardson et al. 2006; Gezer et al. 2020; Boyd et al. 2023).

Previous studies have begun to explore the biological mechanisms mediating these long-lasting effects of developmental dieldrin exposure on the dopaminergic system, but these mechanisms remain incompletely defined (Richardson et al. 2006; Kochmanski et al. 2019; Gezer et al. 2020; Boyd et al. 2023). The primary mechanism of action of dieldrin is thought to be inhibition of GABA_A receptors (Narahashi et al. 1995; Narahashi 1996). Because GABA acts as an important trophic factor in the embryonic and postnatal brain, disruption of these pathways in development is linked to neurodevelopmental and neuropsychiatric disorders; thus, dieldrin inhibition of these GABA-related pathways may affect multiple downstream pathways critical for development (Deidda et al. 2014). However, the mechanisms by which such inhibition leads to persistent effects on neuronal susceptibility remain incompletely defined.

Previously, we showed that developmental dieldrin exposure was associated with significant, sex-specific differential modification of cytosines (DMCs) and regions (DMRs) in genes related to dopaminergic neuron development and PD at 12 wk of age—the time point at which MPTP or α -syn PFFs are administered (Kochmanski et al. 2019). However, these previously reported

changes could be due to either altered establishment of DNA methylation patterns during development and/or disrupted epigenetic aging. Given recent studies showing that environmental factors modify longitudinal trajectories of epigenetic aging, and that age is the primary risk factor for PD, it is critical to determine the longitudinal effects of developmental dieldrin exposure on DNA modifications. (Kochmanski et al. 2017; Barrere-Cain and Allard 2020). By assessing dieldrin-induced changes from birth to 9 mo of age, this study tests if these changes occur early in development and are maintained as the animal ages, and/or if the pattern of change over time is disrupted. To test this, we assessed DNA modifications at multiple time points throughout the life course—birth, 6, 12, and 36 wk old—across the full coding regions of previously identified candidate genes using capture hybridization sequencing (Roche SeqCapEpi). The data reported here reveals potential predegenerative mechanisms by which early-life environmental exposures contribute to late-life risk of PD.

Materials and methods

Animals

Adult female and male C57BL/6 mice (RRID:MGI:2159769) were purchased from Jackson Laboratory (Bar Harbor, Maine). Seven-wk-old female mice were allowed to habituate after arrival for 1 wk prior to beginning the developmental dieldrin exposure. Male mice were 11 wk old upon arrival and were also allowed 1 wk to habituate prior to mating. Mice were maintained on a 12-h:12-h reverse light/dark cycle. Mice were housed in Thoren ventilated caging systems with automatic water and 1/8-in Bed-O-Cobs bedding with Enviro-Dri for enrichment. Food and water were available ad libitum. Mice were maintained on Teklad 8940 rodent diet (Envigo). After arrival, females were separated and individually housed during dieldrin dosing, except during the mating phase. After birth, F1 pups were group-housed by sex, with no more than 5 animals housed in each cage. No singly housed F1 animals were used in this study; as animals aged, all cages included a “buddy” littermate to ensure that even animals used for the last time point were never individually housed. All procedures were conducted in accordance with the National Institutes of Health Guide for Care and Use of Laboratory Animals and approved by the Institutional Animal Care and Use Committee at Michigan State University.

Developmental dieldrin exposure

Dieldrin exposure was carried out as previously described and is summarized in Fig. 1 (Richardson et al. 2006; Kochmanski et al. 2019; Gezer et al. 2020; Boyd et al. 2023). Adult (8 wk old) C57BL/6 female mice ($n = 20$ per group) were treated throughout breeding, gestation, and lactation. Following 3 d of habituation to peanut butter feeding, mice were administered 0.3 mg/kg dieldrin (ChemService) dissolved in corn oil vehicle and mixed with peanut butter pellets every 3 d (Richardson et al. 2006; Kochmanski et al. 2019; Gezer et al. 2020; Boyd et al. 2023). Control mice received an equivalent amount of corn oil vehicle mixed in peanut butter. Mice were exposed via oral ingestion by the dam because the most likely route of exposure to dieldrin in humans is through ingestion of contaminated foods and ingestion of the resulting contaminated breast milk (ATSDR 2022).

The dieldrin dose was based on previous results showing low toxicity, but clear effects on the epigenome and neuronal susceptibility to neurotoxic insults (Richardson et al. 2006; Kochmanski et al. 2019; Gezer et al. 2020; Boyd et al. 2023). In addition, because dieldrin is a persistent compound, even though

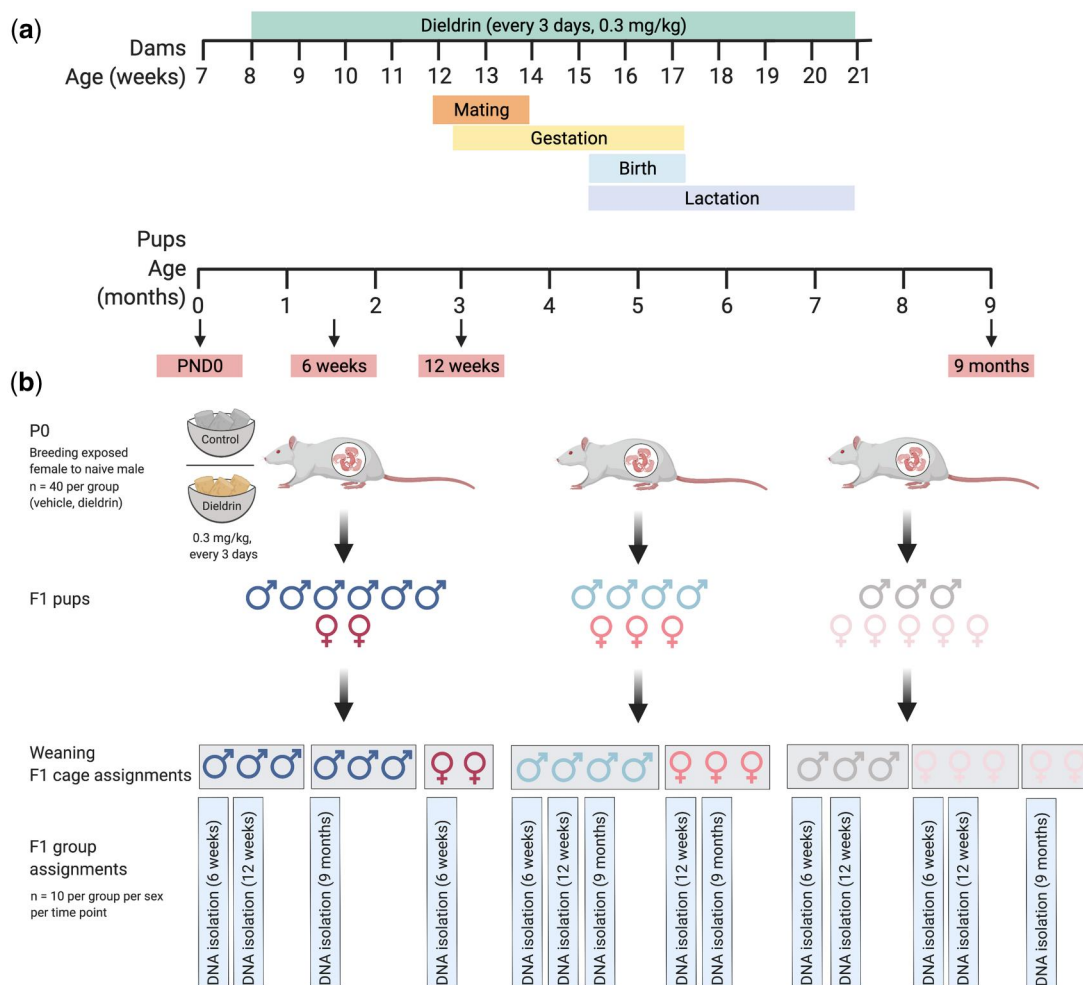


Fig. 1. Dosing timeline, weaning strategy, and cage assignments. a) Timeline of developmental dieldrin exposure model. In this paradigm, only female F0 dams were fed dieldrin. Exposure began at 8 wk of age with 0.3 mg/kg dieldrin dissolved in corn oil vehicle and administered via peanut butter pellets. Males were introduced for mating when females were 12 wk of age (4 wk into exposure). Pregnancy was confirmed by monitoring weight gain after mating. Dieldrin administration continued until pups (F1) were weaned at PND21. F1 pups were sacrificed for brain collection at birth (PND0), 6 wk of age, 12 wk of age, or 36 wk of age. The birth timepoint was collected from one cohort of exposed animals, whereas the remaining three timepoints were collected from a second cohort of exposed animals. b) Weaning strategy and cage assignments for F1 pups followed over time. At weaning, pups (F1) were separated by sex (symbol) and litter (colors represent independent litters) with 2 to 5 animals per cage (grey boxes indicate cages). Animals were assigned to cages such that for each treatment group and sex, all animals were from independent litters and no animals were singly housed. Created in BioRender.

this daily dose is likely higher than human doses, this dose was chosen to produce a similar body burden in animals compared with known levels in humans. There is a very wide range of values reported for both brain (~4 ppb–1 ppm) and adipose (~50 ppb–50 ppm) tissue levels (Fleming et al. 1994; U.S. Environmental Protection Agency 1994; Corrigan et al. 2000; Agency for Toxic Substances and Disease Registry 2022). Our measurements in this cohort in dam brain and adipose tissue are within the reported ranges of multiple studies (Table 1). In this study, we measured these as a quality control step on a subset of animals, but the range of levels between animals suggests that there are variable exposure levels in the pups and that measuring dieldrin in dam and pup tissue in future studies is warranted.

After 4 wk of exposure, unexposed C57BL/6 males (12 wk old) were introduced for breeding for 48 h such that male mice were not present for any peanut butter pellet feedings. To ensure adequate animal numbers for each sex at all four time points, this was carried out in two cohorts: one to generate animals for

Table 1. Dieldrin levels in dam brain and adipose tissue.

Dam brain (ng/g; ppb)	Dam adipose (ng/g; ppb)
24.82	1,659
143.8	7,175
42.08	2,497

Brain and adipose tissue samples were collected from 4 randomly selected dams per treatment group at 20 to 22 wk of age (2 wk after weaning pups and the cessation of exposure). One sample was excluded by Grubb's test as a statistical outlier, leaving 3 dieldrin treated animals. Dieldrin was not detected in samples from vehicle treated animals.

the birth time point, and one to generate animals for the 6-, 12-, and 36-wk time points. For the birth cohort, pups were sacrificed at PND0, tissue was collected for sex determination by genotyping, and whole brains were dissected and frozen. For the remaining cohort, F1 pups were weaned and separated by litter and by sex at 3 wk of age, with 2 to 5 animals per cage. At each time point, male and female littermates from independent litters were

Table 2. Samples sizes for each treatment group by sex at all timepoints.

Age	Female		Male	
	Vehicle	Dieldrin	Vehicle	Dieldrin
Birth	5	7	4	7
6 wk	8	9	10	10
12 wk	8	9	10	9
36 wk	10	10	10	10

selected. Animals were assigned to cages such that for each experimental group and sex, all animals were from independent litters and no animals were singly housed.

Group sizes were determined based on the previously published reduced representation bisulfite sequencing (RRBS) data that this analysis was based (Kochmanski et al. 2019). Based on that data, we determined prior to starting the exposure cohorts that a sample size of at least 7 per sex per treatment group per time point was sufficient to detect >80% of all true differences with an effect size >1.4 (among the smallest effect sizes from our previous data). Samples sizes of 8 to 10 are powered to detect >95% of effects >1.8 (the median effect size from the previous data). At the PND0 timepoint, we only generated 5 female and 4 male control pups and 7 dieldrin exposed pups for each sex from independent litters, limiting our statistical power at birth to 80% power to detect >80% of effects >1.8. We have reported this birth analysis for completeness, but it is important to acknowledge that the statistical power at birth was lower than for other time points for smaller effect sizes. Sample sizes are shown in Table 2.

The 12-wk time point was selected based on previous results demonstrating increased neuronal susceptibility to MPTP and α -syn PFFs administered at 12 wk of age (Richardson et al. 2006; Gezer et al. 2020). The 9-mo time point is equivalent to the 6-mo post-PFF injection time point where we observed dieldrin-induced exacerbation of PFF-induced deficits in motor behavior and DA handling (Gezer et al. 2020). Birth and 6 wk were selected to address the question of whether dieldrin-associated changes reflect a change in establishment or maintenance of epigenetic marks across time.

Sex determination genotyping at birth

At the birth time point, sex determination was not possible by visual inspection and was determined using PCR for *Rmb31x/y* gametologs using an established primer pair (Tunster 2017). DNA was isolated from tail clips taken from neonatal mice during sacrifice using the Kapa Express Extract Kit (Kapa Biosystems, Cat No. KK7100) with one minor modification—sample lysis was assisted via physical homogenization using a 1.5-ml tube plastic pestle. After lysis, samples were briefly centrifuged to pellet cellular debris, and the DNA extract was diluted 10-fold with 10 mM Tris-HCl (pH 8.0 to 8.5) to dilute cellular debris and digested proteins to prevent inhibition of downstream PCR. PCR was performed using 1 μ l of input DNA as described (Richardson et al. 2006; Kochmanski et al. 2019; Gezer et al. 2020; Boyd et al. 2023). PCR products were visualized on a 1.2% Agarose TBE gel with ethidium bromide. During visualization, two bands of DNA were produced for male samples, and a single band of DNA was produced for female samples, allowing for accurate determination of sex at birth.

Mass spectrometry

Dieldrin levels were measured from frozen neonatal brain, dam brain, and dam adipose tissue by the RTSF Mass Spectrometry and Metabolomics core at MSU using established methods (Hong et al. 2004; US Environmental Protection Agency 2014).

SN microdissections

Frozen brains were mounted on a freezing cryostat (Leica, Model CM3050S) and sliced to the midbrain. Unilateral substantia nigra (SN) punches were collected using a chilled 1.0-mm micropunch and immediately placed in a frozen 1.5-ml tube on dry ice.

DNA isolation

DNA was isolated from unilateral SN punches using Qiagen QIAamp DNA Micro Kits (Qiagen, Cat No. 56304) according to the included protocols with the following minor modifications. First, prior to adding ATL buffer to SN punches, 80 μ l PBS was added to each sample and a 1.5-ml tube pestle was used to break up the sample. After that, 100 μ l ATL buffer was added to each homogenized sample, which was allowed to equilibrate to room temperature. Second, for the proteinase K digestion step, the 56 °C incubation time was extended to overnight. Third, carrier RNA was added to Buffer AL (this is an optional step). Fourth, the incubation time after addition of 100% EtOH was increased to 10 min, and the incubation time for the elution step was increased to 5 min. Lastly, to increase yield, the elution step was repeated by reapplying elution buffer to QIAamp MinElute column. DNA was eluted in 54 μ l of 10 mM Tris-HCl, pH 8.0. DNA yield and purity were determined using a Qubit 3 fluorometer (ThermoFisher) and a NanoDrop spectrophotometer (ThermoFisher). Isolated DNA was stored at –80 °C prior to sequencing.

Selection of candidate regions

To select candidate regions, we targeted all intragenic genomic features and known enhancers at genes annotated to DMCs or DMRs in our previous study (Kochmanski et al. 2019). Targeted regions include 255 male-specific annotations and 1,043 female-specific annotations and represent a total of ~11.4 Mb of genomic space (File S1). We included regions identified for both male- and female-specific changes to determine if these are truly sex-specific. Intergenic regions annotated to our candidate genes account for 151 Mb of genomic space, making inclusion cost-prohibitive with the SeqCapEpi platform. In addition, these intergenic regions remain largely unexplored, making data generated from these regions of limited interpretability. SeqCapEpi custom bait probes for regions of interest were designed using the Roche NimbleDesign software (File S2). Baits covered 91.6% of target bases for a total capture space of ~10.4 Mb.

Capture hybridization sequencing

Capture hybridization-sequencing libraries were prepared by the Van Andel Genomics Core from 100 ng of high molecular weight DNA using the Accel-NGS Methyl-Seq DNA Library kit (v3.0) (Swift Biosciences, Cat No. 30024). DNA was sheared following manufacturer's protocol to an average size of 250 bp, and sheared DNA was bisulfite converted using the EZ DNA Methylation-Gold kit (Zymo Research, Cat No. D5005) with an elution volume of 15 μ l. Following adapter ligation, 8 cycles of library amplification were performed. Amplified libraries were pooled in batches of 8 and targeted enrichment of a custom ~11.4 Mb region was performed using Roche SeqCapEpi developer probes and SeqCapHyperEpi workflow starting at step 4.0 with the following modification: the capture was performed using IDT

xGen Universal blockers to replace the SeqCap HE Universal Oligo and SeqCap HE Index Oligo. The postcapture amplification was also adjusted to 11 cycles of amplification and the final extension changed from 30 s to 1 min. The quality and quantity of the finished library pools were assessed using a combination of Agilent DNA High Sensitivity chip (Agilent Technologies, Inc.) and QuantiFluor dsDNA System (Promega Corp.). Sequencing (100 bp, paired end) was performed on an Illumina NovaSeq6000 sequencer using an S4, 200-bp sequencing kit (Illumina Inc.) with 10% PhiX included to improve base diversity. Base calling was done by Illumina Real Time Analysis 3 and output of NextSeq Control Software was demultiplexed and converted to FastQ format with the Illumina *Bcl2fastq* software (version 1.9.0).

Data processing

FastQ files were processed using a slightly modified form of the bioinformatics pipeline previously established by our group to analyze RRBS data (Richardson et al. 2006; Kochmanski et al. 2019; Gezer et al. 2020; Boyd et al. 2023). Command line tools and the open-source statistical software R (version 4.1.2) were used for all analyses. For all sequencing data, the *FastQC* tool (version 0.11.7) was used for data quality control, and the *trim_galore* tool (version 0.4.5) was used for adapter trimming (Andrews 2016; Krueger 2017). During adapter trimming, we used the default minimum quality score and added a stringency value of 6, thereby requiring a minimum overlap of 6 bp. Trimmed CapHyb-seq reads were aligned to the *mm10* reference genome using *bismark* (version 0.19.1) (Krueger and Andrews 2011). Methylation data were extracted from the aligned reads in *bismark* using a minimum threshold of 5 reads to include a CpG site in analysis.

Verification of sequencing coverage

To determine the sequencing coverage across the targeted regions, we used *BedTools Basic Protocol 3* for measuring coverage in targeted DNA sequencing experiments as described (Quinlan 2014). BAM files for each sample obtained from *bismark* were compared with targeted bases (File S2) using the *coverage* and *multicov* functions from *bedtools* (version 2.31.0) to determine the fraction of target bases that were captured and their sequencing depths (Quinlan and Hall 2010). In differential modification analysis, only sites with coverage ≥ 5 in all samples were included in analysis. Of 6,604 target regions, 1,359 remained (21%), for ~ 2.8 Mb of captured sequence.

Differential modification analysis

The *DSS* (version 2.48.0) and *DMRcate* (version 2.14.1) R packages were used to test CapHyb-seq data for differential methylation (Feng et al. 2014; Peters et al. 2015). Given that dieldrin exposure has shown sex-specific effects on the dopaminergic system, all differential modification models were stratified by sex (Richardson et al. 2006; Kochmanski et al. 2019; Boyd et al. 2023). All pups included in modeling were from independent litters. Of note, we refer to DNA modifications, rather than DNA methylation, because our BS-based method does not differentiate between DNA methylation and hydroxymethylation. Although DNA hydroxymethylation plays a critical role in gene expression in the brain and is particularly sensitive to environmental factors, methods for differentiating these marks remain limited and cost-prohibitive, especially across multiple time points (Kochmanski and Bernstein 2020).

Cross-sectional differential DNA modification analysis

To test for DMCs by dieldrin exposure at each cross-sectional timepoint, we used the *DMLtest* function in *DSS* to perform two-group Wald tests. For *DMLtest* modeling, the equal dispersion parameter was set to *FALSE* and smoothing was set to *TRUE*. DMCs were considered significant at false discovery rate (FDR) < 0.05 . To test for DMRs at each timepoint, we combined outputs from the *callDMR* function in *DSS* and the *dmrcate* function in *DMRcate*. For *callDMR* modeling, the *P*-value threshold was set to 0.05, minimum length was set to 50 base pairs, and minimum CpGs was set to 3. Meanwhile, for *dmrcate* modeling, the lambda value was set to 500, the C value was set to 4, and minimum CpGs was set to 3. DMR significance for the *dmrcate* output was set to a minimum smoothed FDR < 0.05 .

Longitudinal differential DNA modification analysis

To test for DMCs by age, as well as simultaneous age and exposure in a multivariate model, we used the *DMLfit.multiFactor* function in *DSS* to perform linear models using a general experimental design. Given that age was an ordered variable, we coded each age group as a number for modeling—6 wk old = 1, 12 wk old = 2, and 36 wk old = 3. The birth timepoint was not included in longitudinal models because the F1 offspring came from a separate cohort of exposed animals, meaning they were not matched littermates like the later three time points. In the model for age only, coded age was included as the only independent variable. Meanwhile, in the multivariate model, exposure was included as a two-group categorical variable (“dieldrin,” “control”), and age:exposure was included as an interaction term. For the age alone and age:exposure models, DMCs were considered significant at FDR < 0.05 .

Genomic annotation

After differential methylation testing, the *annotatr* R package (version 1.26.0) was used to annotate identified DMCs and DMRs to the reference *mm10* genome (Cavalcante and Sartor 2017). Within *annotatr*, the *annotate_regions* function was used to generate CpG context, gene body, and regulatory feature annotations. Annotations for miRNA (miRbase), ENCODE predicted mouse midbrain enhancers (Accession: ENCSR114ZII), and custom full-stack ChromHMM chromatin states for *mm10* databases were added to the annotation cache in *annotatr* (Kundaje et al. 2012; Kozomara et al. 2019; Luo et al. 2020; Vu and Ernst 2023).

Data visualization

Raw CapHyb-seq beta values were extracted using the *bsseq* R package (1.36.0). Volcano plots were generated using the *ggplot2* R package (version 3.4.4). Euler diagrams were generated with the *eulerr* R package (version 7.0.1) (Larsson 2024). UpSet plots were generated using the *UpSetR* package (version 1.4.0) (Conway et al. 2017). The *ComplexHeatmap* R package (version 2.18.0) was used to visualize beta value differences over time for all DMCs significant at one or more of the four time points. Specific genes of interest were visualized using the WASHU Epigenome Browser to determine the genomic location and context of differentially modified (DM) regions; chromHMM annotations were loaded to compare DM loci with chromatin state annotations (Conway et al. 2017; Li et al. 2022). The R packages *ggplot2*, *ggpubr* (version 0.6.0), and *ggeasy* (version 0.1.4) were used to generate violin plots to display raw beta values for premature aging DMCs (Carroll et al. 2023; Kassambara 2023).

Pathway and network analysis

Gene ontology (GO) term enrichment testing and pathway analysis were performed on genes annotated to male and female DMCs and DMRs using the ClueGO application in Cytoscape (version 3.10.1) (Bindea et al. 2009; Smoot et al. 2011).

For ClueGO testing, genes annotated to DMCs and DMRs stratified by sex and timepoint were input as separate gene lists, “groups” was selected as the visual style, and the GO-biological process (GOBP) term was included for enrichment testing. Network specificity was set to “Medium,” such that the GO Tree Interval minimum was equal to 3 and the maximum was equal to 8. Only terms with at least 3 genes and a Bonferroni-corrected *P*-value <0.05 were included in pathway visualizations. The connectivity score (Kappa) was set at 0.4, and default GO Term Grouping settings were used in all analyses. The genes found in enriched GOBP terms by ClueGO were used for STRING network analysis and to create UpSet plots for each sex displaying the overlap at different time points.

Protein–protein interaction network analysis was performed using STRING (version 12.0) with the genes found in enriched GOBP terms by ClueGO as input (Szklarczyk et al. 2015, 2017). STRING network analysis was performed using default parameters, including a minimum required interaction score = 0.4 and all interaction sources activated.

All code and metadata used for these analyses are provided in Files S13–S20.

Results

Cross-sectional analysis of DNA modifications

In our first stage of analysis, we stratified data by sex and identified diethylstilbestrol-associated significant DMCs and DMRs at each assessed time point. DMCs and DMRs results are summarized in Table 3 and DMCs are summarized in Fig. 2a–c. The large majority of the intragenic DM loci are found within introns, as expected based on genomic space (Fig. 2e). The majority of DM loci are found in regions annotated by chromatin state analysis as active enhancers, with weak enhancers and promoters as the next two most frequent categories (Fig. 2f). Complete cross-sectional results and annotations are included in Files S3–S7. The numbers of genes containing DMCs or DMRs were determined after annotation and are summarized in Table 4. There are far fewer genes containing DMCs and DMRs indicating that each gene contains multiple sites of differential modification (Fig. 2c and d). To

Table 3. Numbers of identified DMCs and DMRs associated with diethylstilbestrol exposure in each sex at each time point.

	DMCs		DMRs	
	Female	Male	Female	Male
Birth	2,323	1,629	125	96
Hypermodification	1,613	876	97	45
Hypomodification	710	753	28	51
6 wk	2,547	1,452	130	70
Hypermodification	1,834	998	97	51
Hypomodification	713	454	33	19
12 wk	1,969	1,079	101	44
Hypermodification	1,244	688	59	26
Hypomodification	725	391	42	18
36 wk	976	1,044	31	46
Hypermodification	703	718	19	28
Hypomodification	273	326	12	18

generate gene lists for subsequent analysis, we identified unique gene lists for each sex and time point (File S8).

We also identified genes that containing diethylstilbestrol-associated DMCs or DMRs at all time points for each sex (Fig. 3). For all genes, 63 and 49 genes were DM at all time points in female and male animals, respectively, with 33 shared genes between sexes at all time points (Fig. 3a and b). For genes included in enriched GO terms, only 10 genes were DM at all time points for female animals and only 7 for male animals. Only 4 were DM at all time points in both sexes (*Ephb2*, *Fgfr2*, *Foxp1*, *Prkca*) (Fig. 3c and d). Genes DM and found within enriched GO terms at all time points in male animals, but not female animals, include *Gnas*, *Myo3b*, and *Sbno2*. Genes DM and found within enriched GO terms at all time points in female animals, but not male animals include *Grb10*, *Hoxa2*, *Lmna*, *Ptk7*, *Rhoq*, and *Xylt1*. At each time point for each of these genes, the location of DMCs and DMRs are largely inconsistent, indicating that the differential modification of these genes is complex and dynamic with sex, age, and location-specific changes.

To explore if there are clear patterns over time by specific location, we generated heatmaps of all significant diethylstilbestrol-associated DMCs clustered by patterns in the direction of change at each time point, with DMCs hypomodified at all time points at the bottom and those hypermodified at all time points at the top (Fig. 4). We observed an overall decline in the number of both DMCs and DMRs with increasing age in both male and female animals (Fig. 2a and b, Table 3). In addition, we observed a skew in the number of DMCs/DMRs toward increased modification in both sexes at all time points, whereas DMCs/DMRs at birth in male animals were more evenly split by direction of change. Heatmaps show changes in beta value difference over time, but there is not an overall, consistent indication at this level of analysis that diethylstilbestrol is causing global deficits in establishment or maintenance of epigenetic marks or an acceleration epigenetic aging (Fig. 4).

Functional annotation of DM genes

To determine if diethylstilbestrol-associated DM genes function in known pathways and networks, we generated unique gene lists from annotated DMC and DMR data for each sex and time point for downstream analysis (File S8). From each list, GO term enrichment analysis was performed in ClueGO (Tables S1 and S2). Genes within enriched GO terms were used as input for STRING network analysis to identify potential functional interactions between genes. Because the genes in these networks were overlapping across timepoints, networks for all time points group together are shown in Fig. 5, whereas networks for each separate time point are shown in Fig. S1. For female data, of the 73 genes in enriched GO terms, 43 genes were included in a highly interconnected network. Similarly, for male data, of the 85 genes in enriched GO terms, 47 genes were included in a highly interconnected network. That these genes are highly interconnected was expected because these genes were selected for this analysis based on shared GO terms and potential interactions in STRING in our previous study (Kochmanski et al. 2019).

Selection and characterization of candidate genes

From the large list of diethylstilbestrol-associated DM genes, we selected candidate genes to highlight with related functions in key pathways based on confirmed expression in midbrain/SN, connections in GO term and STRING analyses, and a priori knowledge of these genes (Fig. 5, Table 5, Tables S1 and S2). These include genes involved in dopamine neurogenesis and the differentiation

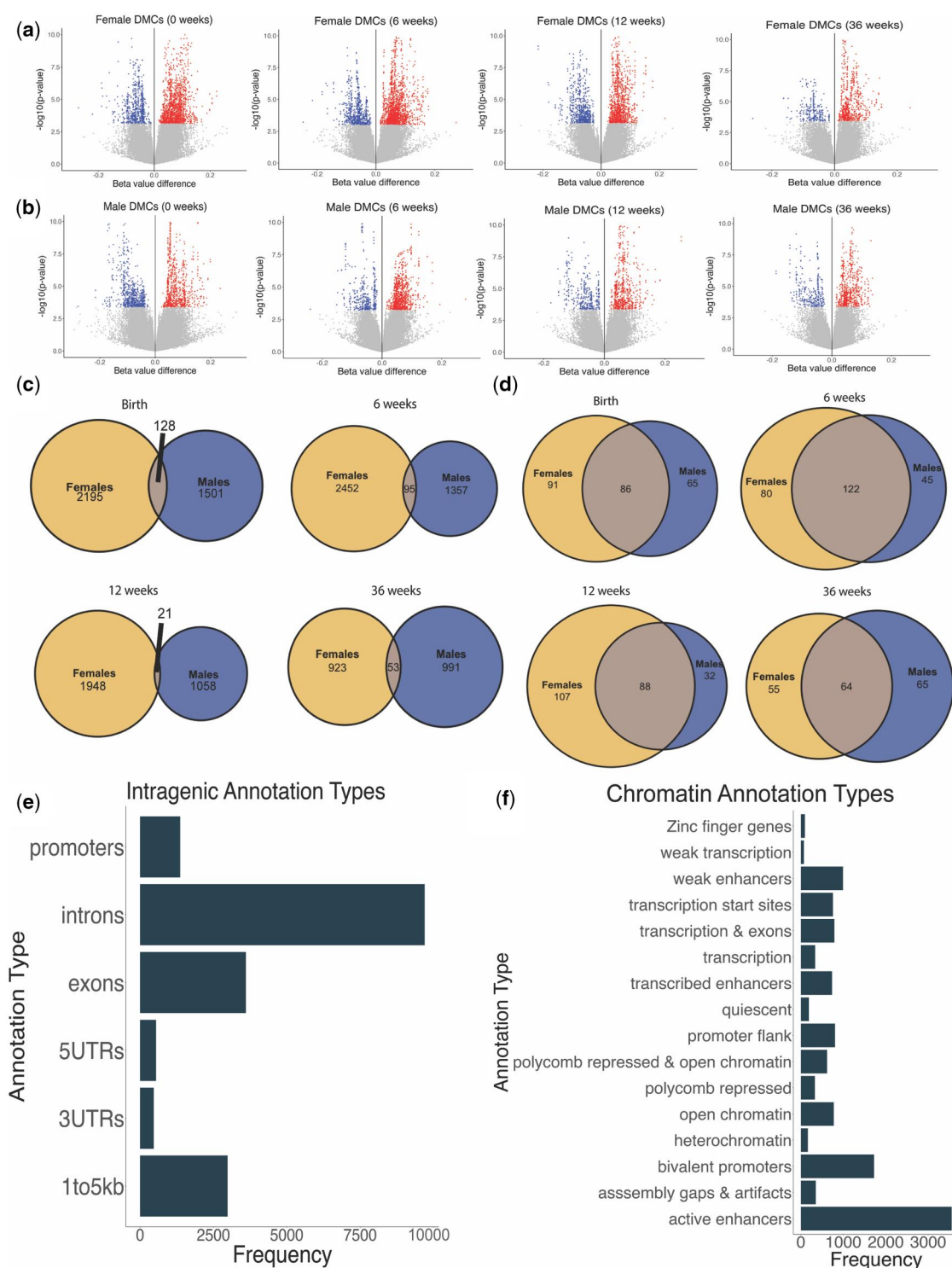


Fig. 2. Significant dieldrin-associated DMCs for each sex at each time point. (a, b) Volcano plots of DMCs for (a) female animal, and (b) male animals at each time point. Beta value differences, plotted on the x-axis, represent the difference between mean methylation values for the control groups from the mean methylation values for the dieldrin groups, such that positive values indicate hypermodified cytosines in exposed animals and negative values indicate hypomethylated cytosines in exposed animals. Colored/dark points represent statistically significant DMCs (FDR < 0.05). Euler diagrams display overlap between sexes at each time of (c) significant DMCs by location or (d) genes containing DMCs or DMRs. Frequency histograms of DMC and DMR annotations for male and female data combined for (e) intragenic annotation types (f) and chromatin annotation types. Annotation numbers are higher than the DMC/DMR numbers because most DMC/DMRs have multiple annotations.

Table 4. Numbers of unique genes annotated to dieldrin-associated DMRs and DMCs.

	DMC genes		DMR genes		Unique genes	
	Female	Male	Female	Male	Female	Male
Birth	176	146	80	51	177	151
Hypermodification	146	103	62	24		
Hypomodification	87	94	23	35		
6 wk	200	162	84	62	202	167
Hypermodification	148	119	61	46		
Hypomodification	105	85	29	19		
12 wk	189	116	78	38	195	120
Hypermodification	138	93	52	26		
Hypomodification	98	52	36	16		
36 wk	119	126	32	36	119	129
Hypermodification	85	90	21	24		
Hypomodification	62	68	11	17		

DMC Genes and DMR Genes columns include unique genes in each category. Many genes have multiple sites of differential modification. The Unique Genes column indicates the number of unique genes annotated to DMCs and DMRs for each sex and time point. These final lists of unique genes for each time point were utilized in downstream analysis steps.

and survival of midbrain DA neurons (*Nr4a2*, *Lmx1b*); fibroblast growth factor signaling (*Fgf8*, *Fgfr2*, *Stat1*); synaptogenesis, maintenance of synaptic structure, and synaptic plasticity (*Ephb2*, *Dlg2*, *Dlgap1*, *Camk2b*, *Prkca*, *Prkce*), epigenetic regulators (*Dnmt31*, *Hdac9*), and two imprinted genes (*Gnas*, *Grb10*).

Overall, we found that candidate gene DMCs and DMRs tend to cluster together and that hypomodified and hypermodified DMCs and DMRs occur together (i.e. these are not interspersed within clusters of differential modifications). Highlighting the sex-specificity and age-dependence of epigenetic regulation, there was limited overlap within these genes between timepoints and sexes in location or direction of change, even in those genes that were identified in both sexes and all timepoints. In addition, consistent with the frequency of DMC/DMR annotations, identified DM loci occur in regions likely to be regulated by differential modifications, including regions annotated by chromHMM as promoters, transcription start sites of major and alternate transcripts, and enhancers (Figs 2 and 6, Files S6 and S7).

In Fig. 6, we used the WashU Epigenome Browser to explore the genomic location and context of dieldrin-associated DMCs and DMRs within the candidate genes. Selected regions are described below and were visualized in the WashU Epigenome Browser to highlight examples of the sex-, age-, and location-specificity of dieldrin-induced differential modifications (Fig. 6) (Li et al. 2022).

Sex- and age-specific differential modifications

Two male-specific nonoverlapping hypermodified DMRs found only at 6 wk and 9 mo annotated to *Lmx1b*, located in a bivalent promoter that drives expression of *Lmx1b* and C130021120Rik, a co-expressed lncRNA (Fig. 6a). Multiple DM loci annotated to *Nr4a2* were identified in female animals at 12 wk and 9 mo and in male animals at 9 mo only. Shown is a female-specific hypomodified DMR in *Nr4a2* found at 12 wk only that spans an exon-intron boundary and maps to a region annotated as a bivalent promoter (Fig. 6b). DMC/DMRs were identified at all timepoints in both sexes in *Ephb2*, and they all map to intron 1. The male-specific hypermodified DMR shown is located within a promoter immediately downstream of the transcription start site and was identified at 12 wk only (Fig. 6c). DM loci annotated within *Prkca* were identified in both sexes at all time points. These map to intron 2 and overlap with a noncoding RNA within this locus.

The female-specific hypermodified DMR shown maps to a region of open chromatin between two enhancers and was identified only at 6 wk (Fig. 6d).

Complex differential modification of imprinted genes

Differential modification of the imprinted genes, *Grb10* and *Gnas*, are highly age-, sex-, and location-specific. DM loci annotated to *Grb10* were identified in both sexes at all time points and all are located within two neighboring CpG islands (Fig. 6e). One hypermodified DMR in female samples at 36 wk is located within the transcription start site. The downstream CpG island contains multiple overlapping DM regions within a bivalent promoter at birth (hyper), 6 wk (hypo), and 9 mo (hyper) in female samples, and at all time points in male samples (hypomodified at birth; hypermodified at 6 wk, 12 wk, and 9 mo). DM regions were identified in the imprinted gene *Gnas* at all time points in both sexes. These are located in all 3 CpG islands/promoters of this gene with no consistent pattern in the direction of change by age, sex, or location (Fig. 6f).

In Table 5, we summarize data on these selected genes, including the time points and sex at which each contained dieldrin-associated DM loci, cell type expression within the SN from the Allen Brain Cell Atlas, and the GO terms each gene mapped to in the ClueGO analysis (Yao et al. 2023). Because the current data are derived from a bulk tissue micropunch, we do not have cell-type-specific data. Thus, we cross-referenced candidate genes to the Allen Brain Cell Atlas to identify genes with known SN expression in mice 7- to 10-wk old, as well as which cell types they are known to be expressed in Yao et al. (2023).

Dieldrin-induced deflection of age-related DNA modification patterns

To determine whether dieldrin deflects long-term trajectories of age-related DNA modification patterns, we first identified DMCs with age-related changes in only control animals at the three time points where data were collected from matched littermates across time—6, 12, and 36 wk old. We identified 290 age-related DMCs in males and 444 age-related DMCs in females (Table 6). Consistent with the cross-sectional analyses, these DMCs were largely sex-specific with only 15 age-related DMCs overlapping between both male and female control animals. Detailed age-related DMCs split by sex are available as supplementary data tables (Files S9 and S10).

To reduce the number of comparisons and preserve statistical power during differential testing across multiple time points, only those cytosines with significant age-related changes were included in subsequent age:exposure interaction modeling. In the age:exposure interaction models, we identified 115 DMCs in female samples and 18 in male samples that had a significant interaction between age and dieldrin exposure (Table 6, Files S11 and S12). Of note, none of these “deflected DMCs” overlapped between the two sexes. Most of these DMCs were not previously identified by the cross-sectional analysis and map to 7 (female) and 3 (male) additional genes.

Next, we compared the direction of change for these “deflected DMCs” from 6 to 36 wk of age to determine if dieldrin led to premature epigenetic aging. Only 1 DMC showed a pattern consistent with premature epigenetic aging. In this scenario, the DMC was hypermodified at 6 by dieldrin, such that the β -value in dieldrin-exposed animals at 6 wk was “prematurely” high and more similar to the β -value in control animals at 36 wk (Fig. 7). In contrast, most of these “deflected DMCs” show a “switching” pattern (i.e. inconsistent direction of change in age-related DNA

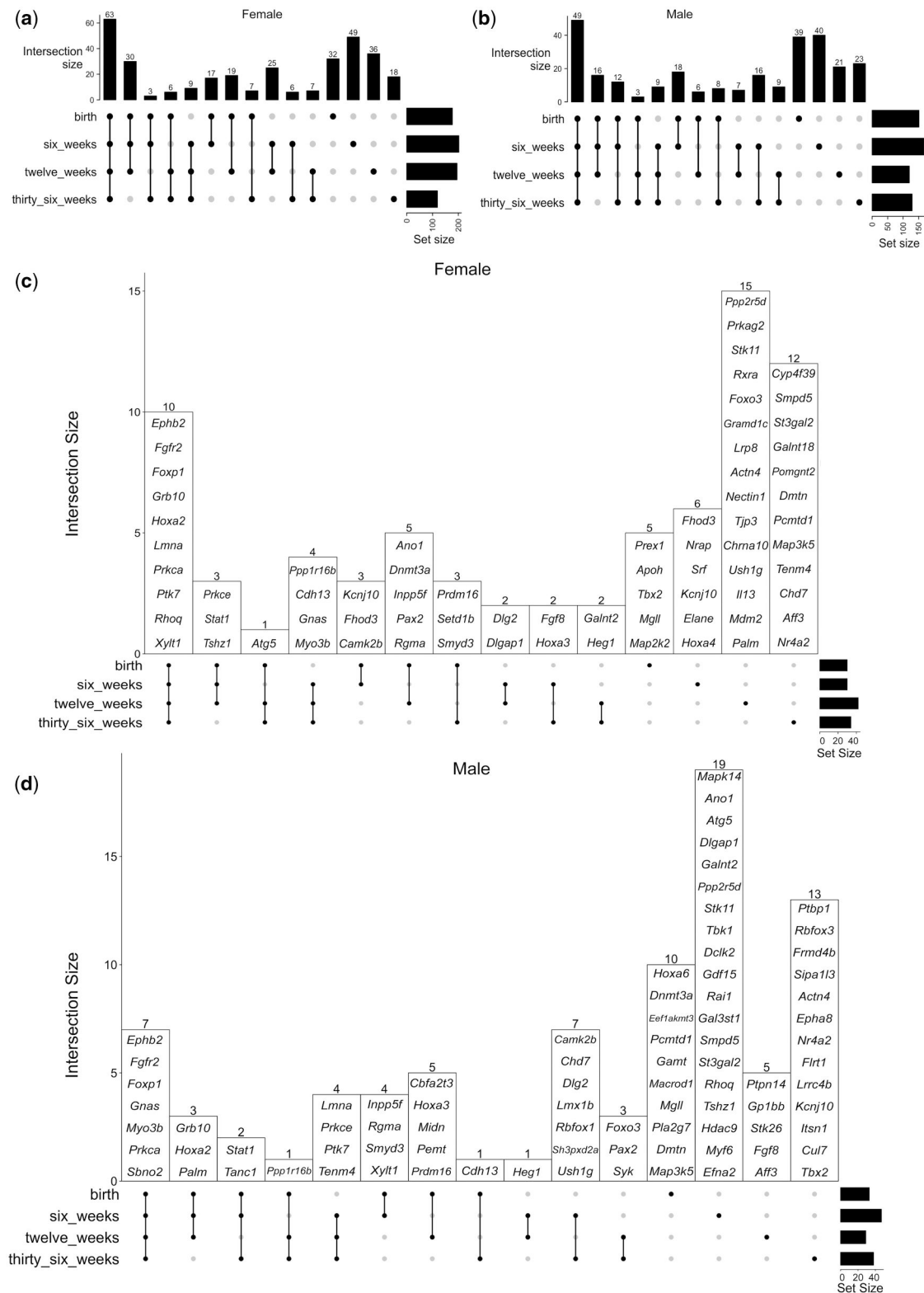


Fig. 3. Overlap between dieldrin-associated differentially modified genes in female and male animals at cross-sectional time points. a, b) UpSet plots show overlap between all differentially modified genes at each time point. c, d) UpSet plots show the overlap between the genes found in enriched GO terms at each time point.

modifications by exposure group) (Table 6). For example, a DMC that is hypermodified at 6 wk in dieldrin-exposed animals but hypomodified at 36 wk, follows a switching pattern (hyper to hypo in Table 6).

Dieldrin is detectable in brains of F1 neonates

In addition to our epigenetic analysis, we tested whether dieldrin was present in the brains of F1 pups at birth. Previous data show that dieldrin is not detectable in the brain of F1 pups at 12 wk of

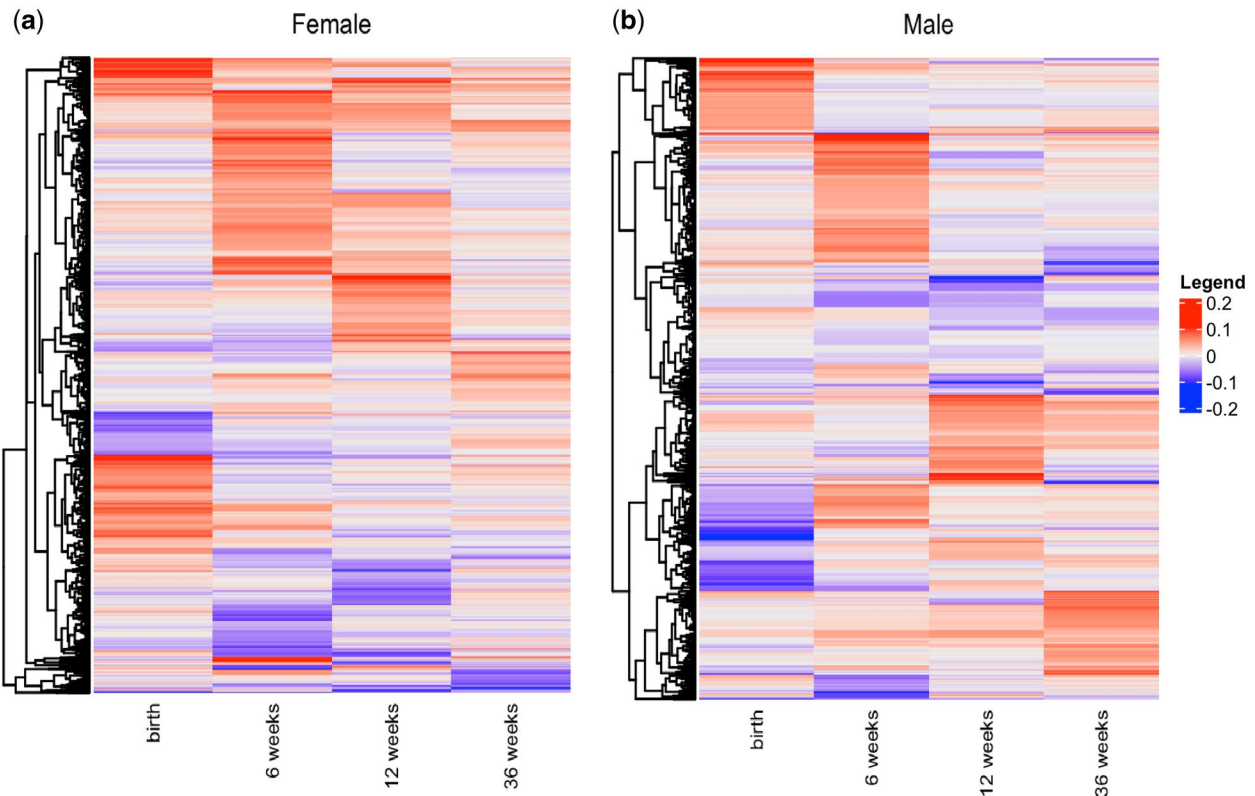


Fig. 4. Beta value differences across cross-sectional time points. Heatmaps display the beta value differences for significant DMCs over time for (a) female animals and (b) male animals. Each row represents a single DMC. Blue indicates hypomodification in dieldrin-exposed animals compared with control and red indicates hypermodification in dieldrin-exposed animals compared with control. Rows are clustered based on the similarity of beta value differences, with DMCs hypomodified at all time points at the bottom and those hypermodified at all time points at the top. A color version of this figure appears in the online version of this article.

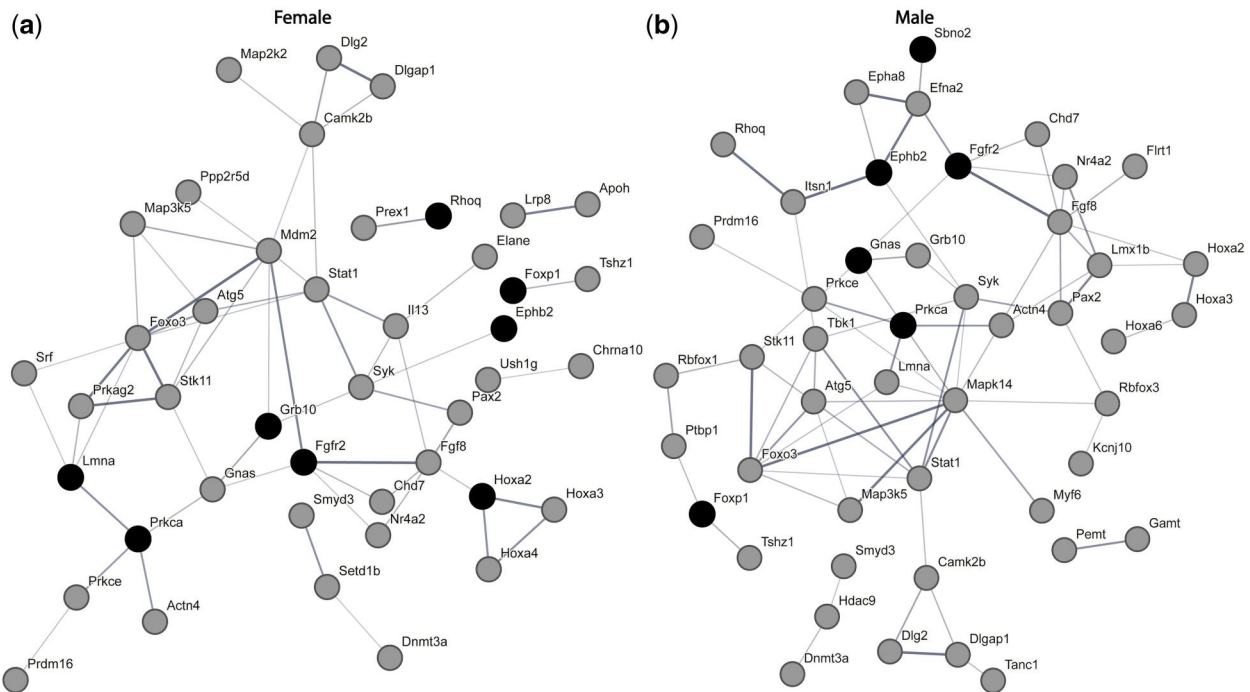


Fig. 5. STRING protein-protein interaction networks between genes found in enriched GO terms. Interaction networks for DM genes from female (a) and male (b) animals at all time points combined. STRING networks display the interactions with at least a 0.4 interaction score and omit any disconnected nodes. Each node represents all proteins produced by a single, protein-coding gene locus. Edges represent protein-protein associations, but not necessarily physical interactions. The thickness of the lines indicates the strength of data support. Genes identified at all time points are highlighted in black.

Table 5. Summary of selected differentially modified genes.

Gene	Female				Male				SN expression				Enriched GO terms
	0	6	12	36	0	6	12	36	Neu	MG	Astro	Oligo	
<i>Dopamine neurogenesis, differentiation, and survival of midbrain DA neurons</i>								*	+++	+	+	+	Chemorensory behavior, central nervous system neuron development, dopaminergic neuron differentiation Central nervous system neuron development, central nervous system neuron axonogenesis, neuron maturation, dopaminergic neuron differentiation
<i>Lmx1b</i>					*				+++	+			
<i>Fibroblast growth factor signaling</i>			*	*				*	+++	+	+	+	Ear morphogenesis, embryonic skeletal system development, embryonic skeletal system morphogenesis, blood vessel remodeling, cranial skeletal system development, positive regulation of stem cell proliferation, hindlimb morphogenesis, embryonic cranial skeleton morphogenesis, embryonic hindlimb morphogenesis, motor neuron axon guidance, cardiac septum development, inner ear morphogenesis, central nervous system neuron development, animal organ formation, specification of animal organ identity, brain morphogenesis
<i>Fgf8</i>	*	*	*	*	*	*	*	*	+++	+++	+++	+++	
<i>Positive regulation of lipase activity, ear morphogenesis, mesenchymal cell proliferation, regulation of mesenchymal cell proliferation, lung morphogenesis, coronary vasculature development, positive regulation of smooth muscle cell proliferation, embryonic skeletal system development, embryonic skeletal system morphogenesis, inner ear morphogenesis, cardiac muscle cell proliferation, cranial skeletal system development, positive regulation of stem cell proliferation, embryonic cranial skeleton morphogenesis, cardiac septum development, cellular response to retinoic acid, ventricular cardiac muscle tissue development, central nervous system neuron development, ventricular cardiac muscle tissue morphogenesis, positive regulation of mesenchymal cell proliferation, animal organ formation, specification of animal organ identity, striated muscle cell proliferation, regulation of cardiac muscle cell proliferation</i>			*	*	*	*	*	+++	+++	+++	+++	+++	Mesenchymal cell proliferation, regulation of mesenchymal cell proliferation, positive regulation of smooth muscle cell proliferation, syncytium formation by plasma membrane fusion, positive regulation of mesenchymal cell proliferation, syncytium formation, tumor necrosis factor-mediated signaling pathway, lipopolysaccharide-mediated signaling pathway
<i>Stat1</i>	*	*	*	*	*	*	*	+++	+++	+++	+++	+++	
<i>Synaptogenesis, maintenance of synaptic structure, neurotransmission, and synaptic plasticity</i>								*	+	+	+	+	Ear morphogenesis, regulation of neuronal synaptic plasticity, filopodium assembly, regulation of filopodium assembly, inner ear morphogenesis, cranial nerve development, central nervous system neuron development, central nervous system neuron axonogenesis, cranial nerve morphogenesis, positive regulation of synapse assembly, regulation of long-term neuronal synaptic plasticity, positive regulation of dendritic spine development, positive regulation of dendrite morphogenesis
<i>Ephb2</i>	*	*	*	*	*	*	*	+++	+	+	+	+++	

(continued)

Table 5. (continued)

Gene	Female						Male						SN expression				Enriched GO terms	
	0	6	12	36	0	6	12	36	Neu	MG	Astro	Oligo	Neu	MG	Astro	Oligo		
	*	*	*	*	*	*	*	*	+++	+	+++	+	+++	+++	+++	+++		
<i>Dlg2</i>								*										Structural constituent of postsynapse, protein localization to cell junction, neuron maturation
<i>Dlgap1</i>		*	*	*	*	*	*	*										Structural constituent of postsynapse, protein localization to cell junction
<i>Camk2b</i>	*	*	*	*	*	*	*	*	+++	+	+++	+++	+++	+++	+++	+++	+++	Positive regulation of lipase activity, structural constituent of postsynapse, regulation of neuronal synaptic plasticity, neuromuscular process controlling balance, regulation of long-term neuronal synaptic plasticity, positive regulation of dendritic spine development, positive regulation of dendrite morphogenesis
<i>Prkca</i>	*	*	*	*	*	*	*	*	+++	+++	+++	+++	+++	+++	+++	+++	+++	Regulation of glucose import, negative regulation of glucose import, positive regulation of smooth muscle cell proliferation, peptidyl-threonine modification, platelet aggregation, negative regulation of glucose transmembrane transport, central nervous system neuron development, central nervous system neuron axonogenesis, regulation of platelet activation, positive regulation of synapse assembly, lipopolysaccharide-mediated signaling pathway
<i>Prkce</i>	*	*	*	*	*	*	*	*	+++	+++	+++	+++	+++	+++	+++	+++	+++	Macrophage activation involved in immune response, mucus secretion, cellular response to alcohol, chemosensory behavior, lipopolysaccharide-mediated signaling pathway
Imprinted genes																		
<i>Grb10</i>	*	*	*	*	*	*	*	*	+++	+	+	+	+	+	+	+	+	Regulation of glucose import, negative regulation of glucose import, negative regulation of glucose transmembrane transport, negative regulation of carbohydrate metabolic process, negative regulation of cellular carbohydrate metabolic process, positive regulation of cold-induced thermogenesis
<i>Gnas</i>	*	*	*	*	*	*	*	*	+++	+++	+++	+++	+++	+++	+++	+++	+++	Embryonic skeletal system development, embryonic skeletal system morphogenesis, cellular response to alcohol, platelet aggregation, cranial skeletal system development, hindlimb morphogenesis, embryonic cranial skeleton morphogenesis, embryonic hindlimb morphogenesis, regulation of cyclase activity, negative regulation of multicellular organism growth, osteoclast differentiation, positive regulation of cold-induced thermogenesis
Epigenetic regulators																		
<i>Dnmt3a</i>	*	*	*	*	*	*	*	*	+++	+++	+++	+++	+++	+++	+++	+++	+++	Protein methyltransferase activity, cellular response to alcohol
<i>Hdac9</i>	*	*	*	*	*	*	*	*	+++	+++	+++	+++	+++	+++	+++	+++	+++	Myotube differentiation

Genes containing DMCs and DMRs that are described in text are listed, with asterisks indicating the time points at which DMCs or DMRs were identified. Genes visualized in Fig. 6 are indicated in bold. Cell-type expression in the substantia nigra from the Allen Brain Cell Atlas are indicated, with +++ indicating high relative expression compared with other cell types, ++ indicating lower relative expression compared with other cell types, and + indicating sparse expression in only a few cells. Enriched GO terms indicate those that contained the gene in our ClueGO enrichment analysis. 0 = FND0, 6 = 6 wk, 12 = 12 wk, 36 = 9 mo, Neu = dopamine neurons, MG = microglia, Astro = astrocytes, oligo = oligodendrocytes.

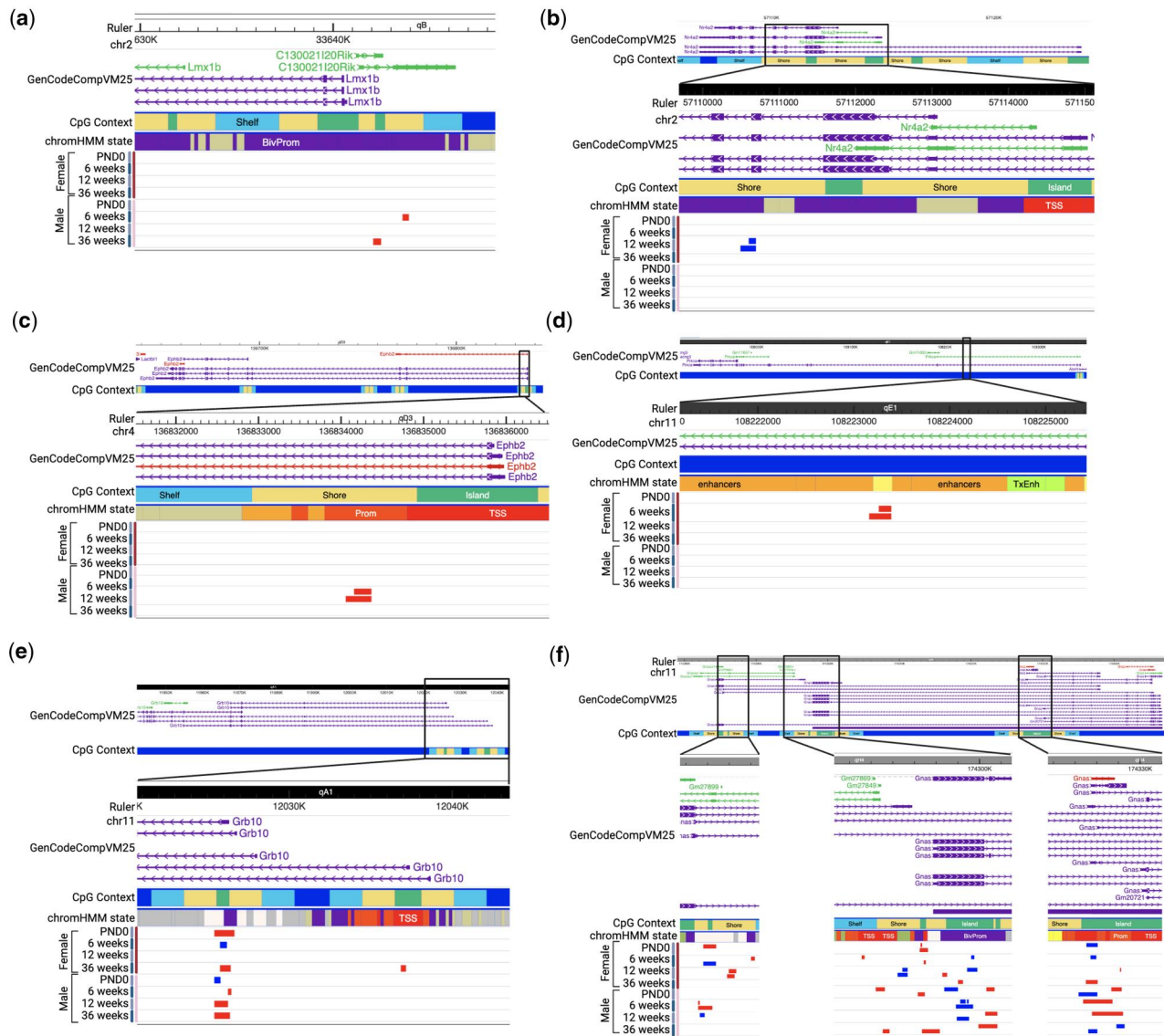


Fig. 6. Visualization of target genes in the Wash U Epigenome Browser. Selected DMRs were visualized in the Wash U Epigenome browser showing CpG context and a ChromHMM track generated from the universal chromatin state annotation for *mm10* (Vu and Ernst 2023). For (b–f), the full genomic locus is shown above; the box indicates the location of the zoomed-in region below. a) A male-specific hypermodified DMR annotated to *Lmx1b* in a bivalent promoter (purple). b) A female-specific hypomethylated DMR annotated to *Nr4a2* spans an exon–intron boundary and maps to a region annotated as a bivalent promoter (purple). c) Male-specific overlapping DMRs in *Ephb2* are found in a promoter flanking region (orange); the direction of change is different at birth and 12 wk. d) A DMR within intron 2 of *Prkca* maps to an active enhancer (light orange) and the direction of change is opposite in male and female samples. A neighboring female-specific hypermodified DMR was identified at 6 wk only. e) DM loci annotated to *Grb10* are located within two neighboring CpG islands in a bivalent promoter (purple) and transcription start site (TSS; red) in a highly sex-, age-, and location-specific manner. f) DM regions in *Gnas* are located in all 3 CpG islands/promoters of this gene with no consistent pattern in the direction of change by age or location. Color coding for GenCode annotation: Purple—coding, Green—noncoding, Red—problem transcript. Color coding for CpG context: Green—CpG island, yellow—shore, light blue—shelf. Color coding for chromHMM state: Purple—bivalent promoter; bright orange—promoter flanking, light orange—active enhancer, red—transcription start site. Color coding for DMRs: Blue indicates hypomethylation; red indicates hypermethylation. A color version of this figure appears in the online version of this article.

age in this exposure paradigm (Richardson et al. 2006). However, dieldrin can cross the placenta and the blood–brain barrier, so we expect dieldrin to be present in the brain during the exposure period. Therefore, to test if dieldrin crosses the placenta and enters the developing brain, we collected brain tissue from extra male F1 neonates ($n = 4$ per group) from independent litters and measured dieldrin levels by mass spectrometry. Raw and processed mass spectrometry data are available in Files S21–S23. As expected, dieldrin was detectable in dieldrin-exposed pups but not in vehicle-exposed pups, with a mean level of 621.9 ng dieldrin/g tissue in dieldrin-exposed offspring (Fig. 8). Given previous

estimates of the half-life of dieldrin in mouse at 1 to 10 d and approximately 3 d in mouse brain, our data that dieldrin is detectable in neonatal brain is consistent with previous data showing the dieldrin is not detectable by 12 wk of age, which is 9 wk after the end of the exposure period (WHO-IPCS 1989; Richardson et al. 2006; Hatcher et al. 2007). Here, we only analyzed male pups based on pups that were available after assigning pups to endpoints to confirm that dieldrin was present in brain at PND0, as this had not previously been reported in this model. However, given the consistent sex differences observed both in dieldrin-exposed animals and in our two-hit model, it is

Table 6. Age-related and deflected DMCs.

Direction	Female	Male	
Age-related DMCs			
Hypermodified	152	89	
Hypomodified	292	201	
Total	444	290	
Deflected DMCs			
Hyper to hypo	81	15	Switch
Hypo to hyper	33	3	
Hyper to hyper	1	0	Premature aging
Hypo to hypo	0	0	

Age-related DMCs have differential modification between 6 and 36 wk, detected using the DSS R package; FDR < 0.05. Deflected DMCs are age-related DMCs with a significant interaction between age and exposure, detected using the DSS R package; FDR < 0.05.

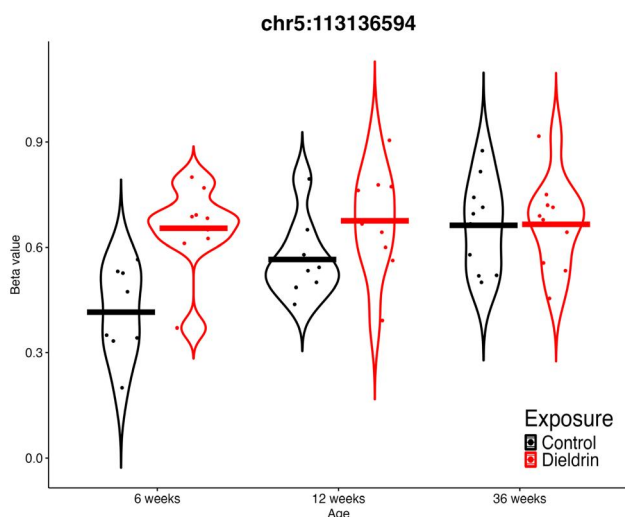


Fig. 7. Raw beta values of the premature aging DMC. Violin plot displays the raw beta values for control and dieldrin female samples at 6, 12, and 36 wk for the deflected DMC that shows patterns consistent with premature epigenetic aging located at chromosome 5, position 113136594. Each point represents a single sample. The horizontal crossbars indicate the mean.

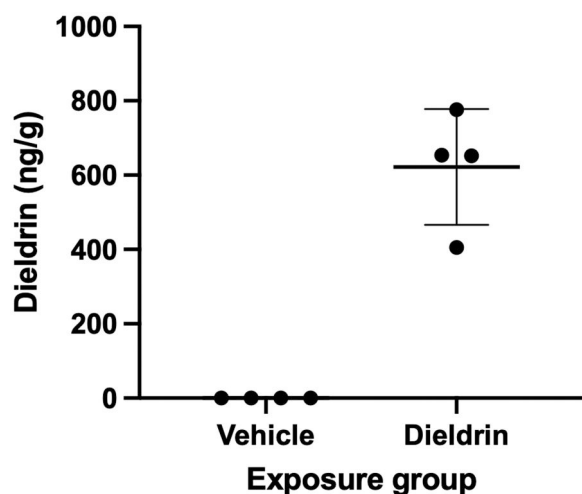


Fig. 8. Dieldrin levels in F1 neonatal brain. Dieldrin levels in neonatal brain from vehicle- and dieldrin-exposed male F1 animals. Data are shown as mean \pm SD.

possible that these sex differences are due to differential accumulation of dieldrin in the developing brains of male and female pups. As with the levels of dieldrin in dam tissue, this suggests that future studies should measure dieldrin in both dam and pup tissue.

Discussion

Dieldrin-induced differential modifications occur within genes with critical functions in neurodevelopment and in maintenance of neurological function

Our findings reinforce the concept of silent neurotoxicity, where the effects of developmental exposures are unmasked by challenges later in life, the cumulative effects of exposures over the lifespan, or the effects of aging (Cory-Slechta et al. 2005; Kraft et al. 2016). The epigenetic changes identified implicate potential mechanisms by which dieldrin primes the nigrostriatal system to have an exacerbated response to PD-related toxicity without observable changes in typical markers of nigrostriatal dysfunction and degeneration. The identification of dieldrin-associated DNA modifications in genes with critical roles in neurodevelopmental pathways and proper neurological function postnatally and into adulthood supports our hypothesis that developmental dieldrin exposure epigenetically regulates specific essential developmental programs and pathways with impacts that persist throughout the lifespan (Table 5, Figs 5 and 6). Here, we highlight specific DM genes and pathways that may be important mediators of the persistent effect of dieldrin exposure (Fig. 6, Table 5, Files S6 and S7).

Two DM genes, *Lmx1b* and *Nr4a2* encode transcription factors involved in the development, maintenance, and survival of DA neurons, and in PD specifically (Decressac et al. 2013; Arenas et al. 2015; Doucet-Beaupré et al. 2015; Oliveira et al. 2017; Jakaria et al. 2019; Al-Nusaif et al. 2022; Gamit et al. 2023; Lim et al. 2024). Further, in our data, multiple components of fibroblast growth factor signaling (*Fgf8*, *Fgfr2*, and *Stat1*) are DM. FGF signaling plays important roles in multiple aspects of neurodevelopment and neurological function in the developing and adult brain, including growth and patterning of the developing brain, neurogenesis, gliogenesis, axon outgrowth, myelination, tissue repair, synaptogenesis, synapse maturation, astrocyte-mediated synaptic pruning, and the maintenance of glia-neuron interactions (Stevens et al. 2010, 2023; Scheltinga et al. 2013; Dabrowski et al. 2015; Klimaschewski and Claus 2021). Supporting the idea that synaptogenesis pathways are affected by early-life dieldrin exposure, additional DM genes have known functions related to synaptogenesis, the maintenance and function of synapses, and synaptic plasticity, including *Ephb2*, *Dlg2*, *Dlgap1*, *Camk2b*, *Prkca*, and *Prkce* (Slonowski and Ethell 2012; Luderman et al. 2015; Kania and Klein 2016; Sen et al. 2016; Rasmussen et al. 2017; Assali et al. 2021; Bu et al. 2021; Liu et al. 2022; Borghi et al. 2023; Südhof 2023; Kaizuka and Takumi 2024). Together, these pathways coordinate the formation, structure, function, and plasticity of synapses across the lifespan, consistent with the idea that the integrity of synapses is critical for proper neurotransmission and that multiple PD-related mechanism converge on disruption of synaptic function (Alter et al. 2013; Soukup et al. 2018; Brooker et al. 2024).

Given the well-documented roles of these genes in these processes, dieldrin-induced changes in epigenetic regulation over time in these genes could contribute to altered susceptibility of the dopaminergic system. It is possible that the observed

alterations in genomic and temporal patterns of DNA modifications in these genes change how gene expression is regulated longitudinally, with differing effects on function over time. In addition, we identified dieldrin-induced changes in epigenetic regulators themselves, providing a potential mechanism by which epigenetic regulation could be disrupted. These data do not yet explore how this epigenetic regulation affects the expression of these genes over time or in response to a parkinsonian insult. Future studies will determine if epigenetic regulation of these loci affects gene expression and transcript usage overtime at the RNA and protein levels, as almost all these highlighted genes have multiple promoters and/or transcripts. In addition, we can utilize our two-hit dieldrin/PFF model to elucidate mechanisms by which those epigenetic changes impact the regulation of expression of these genes in a PD-related model.

DM genes play important roles in glial cell function and neuroinflammation

Importantly, many of the identified dieldrin-associated DM genes highlighted above have known expression and functions in glial cells and in neuroinflammatory processes (Table 5). For example, FGF signaling mediates glia–neuron interactions, including those between oligodendrocytes and axons that are critical for myelination and between astrocytes and synapses for synaptic pruning and plasticity (Klimaschewski and Claus 2021; Stevens et al. 2023). Along with its roles in neuron–neuron signaling, recent evidence shows potential proinflammatory roles for EPHB2 in multiple types of glial cells, possibly via activation by TNF- α /NF- κ B (Pozniak et al. 2014; Yang et al. 2018; Darling and Lamb 2019; Ernst et al. 2019). NF- κ B has been well-studied in PD and has emerged as a potential mediator in the effects of toxicant exposures on neuroinflammation in PD (Anderson et al. 2018). Together, these results add to the rapidly growing recognition of the multifaceted functions of astrocytes, microglia, oligodendrocytes, and other nonneuronal cells, and highlights the need for additional studies into the role of glial cells and neuroinflammation in the response to neurotoxicants and PD.

An important caveat of these findings is that this study does not address the biological significance of these epigenetic changes. While changes in DNA modifications may potentially impact the binding of proteins that regulate gene expression and/or other epigenetic marks, this study does not examine these functional impacts. However, it does provide multiple avenues for further study of the impact of these changes on gene expression, alternate promoter usage, differential isoform expression, and neuronal function and susceptibility. Follow-up studies in our lab are ongoing to test these functional connections.

Distinct sex-specific responses to exposures may underlie sex-specific differences in disease

The reported dieldrin-associated epigenetic changes are largely sex-specific, adding to a growing body of evidence that sex differences in PD could be due to sex-specific responses to PD-related toxicants (Richardson et al. 2006; Kochmanski et al. 2019; Gezer et al. 2020; Adamson et al. 2022). Sex dimorphisms in PD incidence are well-documented, as is a male-specific relative vulnerability to PD-related toxicants (Dluzen and McDermott 2000; Van Den Eeden et al. 2003; Haaxma et al. 2007; Gillies et al. 2014; Georgiev et al. 2017; Jurado-Coronel et al. 2018; Cerri et al. 2019; Adamson et al. 2022). Multiple mechanisms have been proposed as putative mediators of these sex-specific effects, including but not limited to sex differences in glial cell function and immune response (Gillies et al. 2014; Jurado-Coronel et al. 2018; Adamson

et al. 2022). In line with this, our previous study identified sex-specific effects of dieldrin on neuroinflammatory gene expression and the data here expand on that with sex-specific effects on DNA modification in genes with critical functions in glia (Gezer et al. 2020). More generally, these data add to evidence of the sex-specific nature of epigenetic responses to developmental exposures, reiterating the importance of considering sex when investigating the epigenetic mechanisms driving disease development (McCabe et al. 2017; Hilz and Gore 2022; Svoboda et al. 2022a).

Dieldrin induces age- and location-specific changes in DNA modifications

In addition to the sex-specificity of dieldrin-induced differential modification, our data highlight the age- and location-specificity of DNA modifications (Fig. 6). By using capture hybridization-sequencing, we were able to gain a more complete map of DNA modifications across modified genes identified in a previous study in our group; these data show that even within one gene, the direction of change is highly dependent on the specific location (Kochmanski et al. 2019). In addition, the inclusion of multiple time points demonstrates that the position and direction of differential modifications are highly dependent on age. In particular, the imprinted genes, *Grb10* and *Gnas*, provide clear examples of the sex-, age-, and location-specificity of differential modifications (Fig. 6). Overall, dieldrin-associated alterations in the direction and location of the epigenetic regulation of these loci over time may alter gene expression, promoter usage, or isoform expression of these genes differently at different ages. In contrast to the variability in the location and direction of dieldrin-associated epigenetic changes, the overall pathways that are epigenetically dysregulated by dieldrin exposure are quite consistent. The connectivity of the pooled networks in Fig. 5 compared with the individual networks at each time point highlights that the same pathways are being epigenetically regulated in distinct but overlapping patterns over time. These findings underscore the complexity of epigenetic regulation and the importance of studying the effects of exposures longitudinally, as the epigenetic regulation of these genes changes over time.

According to both the multiple hit and stochastic acceleration hypotheses of PD pathogenesis, an accumulation of factors accelerates the normal pace of dopaminergic neuron dysfunction and loss with age, eventually exceeding a threshold for PD development (Sulzer 2007; Collier et al. 2011). The highly age-dependent nature of our results is consistent with these hypotheses and highlight the need for large-scale longitudinal studies in models of chronic effects of exposures to identify biological mechanisms underlying these interactions between aging, environmental exposures, and genetics. Such studies are needed to identify specific epigenetic and gene regulatory changes underlying the age-related biological and pathogenic pathways associated with disease.

Dieldrin exposure does not induce large-scale deflection of long-term trajectories of age-related DNA modification patterns

To specifically test if developmental dieldrin exposure disrupts patterns of epigenetic aging within target genes, we performed an additional analysis of age-related changes. Contrary to the environmental deflection hypothesis, our analysis identified very few DMCs with dieldrin-associated deflection of age-related trajectories (Table 6) (Kochmanski et al. 2017). While this suggests that dieldrin may not be causing large-scale deflection of age-

related trajectories in DNA modification patterns, this is at odds with the age-related differences identified in our cross-sectional analysis and multiple issues limit such a broad interpretation. First, this could be due to statistical differences in how variance is calculated for these two tests within the *DSS* package, which would explain why we found few age-related changes identified in control animals. Second, the birth time point was not included in this analysis because (i) the birth time point was collected from a different cohort and (ii) because neonatal brains are much smaller, these microdissections are quite different. We would expect to see more age-related changes from birth to 36 wk, but these experimental issues complicate the interpretation of that comparison. Third, because we used a targeted method to look at a small fraction of the genome, we may have missed many age-related changes. A genome-wide survey of epigenetic modifications would likely provide a better assessment of age-related changes on which to base this analysis of potential environmental deflection. Finally, this analysis omits DMCs without age-related change in control animals but with age-related change in dieldrin animals. However, limiting the analysis here was critical to preserve statistical power. Overall, it is difficult to make broad conclusions from these data, and the potential interaction between developmental exposure and epigenetic aging warrants further investigation.

Acknowledgments

The authors thank MA and the Van Andel Genomics Core for providing consultation, library preparation, and next-generation sequencing facilities and services (RRID: SCR_022913). They also thank Cassandra Johnny and the Michigan State University Mass Spectrometry and Metabolomics Core for providing mass spectrometry services. They also thank Daofeng Li from Washington University in St Louis for creating a mouse ChromHMM track at our request for the WashU Epigenome Browser.

Author contributions

Joseph Kochmanski: Conceptualization, Methodology, Software, Formal analysis, Visualization, Investigation, Data curation, Writing—original draft; Mahek Virani: Software, Validation, Formal analysis, Data curation, Writing—review & editing, Visualization; Nathan C. Kuhn: Software, Formal analysis, Investigation; Sierra L. Boyd: Investigation; Marie Adams: Investigation, Methodology; Katelyn Becker: Investigation; Alison I. Bernstein: Conceptualization, Methodology, Data curation, Writing—review & editing, Supervision, Project, Visualization, Administration, Funding acquisition.

Supplementary material

[Supplementary material](#) is available at *Toxicological Sciences* online.

Funding

This work was supported by the National Institute of Environmental Health Sciences of the National Institutes of Health under award F32 ES031426 (JK) and R01 ES031237 (AIB).

Conflicts of interest

None declared.

Data availability

Preregistration: <https://doi.org/10.17605/OSF.IO/3QXFV>. Raw sequencing data: GEO Accession No. GSE264165 (reviewer token: axqxaucurtkndmf). All code, processed data, and supporting data are available as [Supplementary Files](#) in the Dryad Data Repository: <https://doi.org/10.5061/dryad.ffbg79d30>.

References

- Adamson A, Buck SA, Freyberg Z, Miranda BRD. 2022. Sex differences in dopaminergic vulnerability to environmental toxicants – implications for Parkinson’s disease. *Curr Environ Health Rep.* 9 (4):563–573.
- Agency for Toxic Substances and Disease Registry (ATSDR). 2022. Toxicological profile for aldrin and dieldrin. Atlanta (GA): U.S. Department of Health and Human Services, Public Health Service.
- Allis CD, Jenuwein T. 2016. The molecular hallmarks of epigenetic control. *Nat Rev Genet.* 17(8):487–500.
- Al-Nusaif M, Yang Y, Li S, Cheng C, Le W. 2022. The role of NURR1 in metabolic abnormalities of Parkinson’s disease. *Mol Neurodegener.* 17(1):46.
- Alter SP, Lenzi GM, Bernstein AI, Miller GW. 2013. Vesicular integrity in Parkinson’s disease. *Curr Neurol Neurosci Rep.* 13(7):362.
- Anderson FL, Coffey MM, Berwin BL, Havrda MC. 2018. Inflammasomes: an emerging mechanism translating environmental toxicant exposure into neuroinflammation in Parkinson’s disease. *Toxicol Sci.* 166(1):3–15.
- Andrews S. 2016. FastQC: a quality control tool for high throughput sequence data. Babraham Institute. <https://www.bioinformatics.babraham.ac.uk/projects/fastqc/>
- Arenas E, Denham M, Villaescusa JC. 2015. How to make a midbrain dopaminergic neuron. *Development.* 142(11):1918–1936.
- Assali A, Cho JY, Tsvetkov E, Gupta AR, Cowan CW. 2021. Sex-dependent role for EPHB2 in brain development and autism-associated behavior. *Neuropsychopharmacology.* 46 (11):2021–2029.
- Barrere-Cain R, Allard P. 2020. An understudied dimension: why age needs to be considered when studying epigenetic-environment interactions. *Epigenet Insights.* 13:2516865720947014.
- Bianco-Miotto T, Craig JM, Gasser YP, Dijk SJV, Ozanne SE. 2017. Epigenetics and DOHaD: from basics to birth and beyond. *J Dev Orig Health Dis.* 8(5):513–519.
- Bindea G, Mlecnik B, Hackl H, Charoentong P, Tosolini M, Kirilovsky A, Fridman W, Pagès F, Trajanoski Z, Galon J. 2009. ClueGO: a cytoscape plug-in to decipher functionally grouped gene ontology and pathway annotation networks. *Bioinformatics.* 25 (8):1091–1093.
- Bogers JS, Bloem BR, Heijer JMD. 2023. The etiology of Parkinson’s disease: new perspectives from gene-environment interactions. *J Parkinsons Dis.* 13(8):1281–1288.
- Borghi R, Trivisano M, Specchio N, Tartaglia M, Compagnucci C. 2023. Understanding the pathogenetic mechanisms underlying altered neuronal function associated with CAMK2B mutations. *Neurosci Biobehav Rev.* 152:105299.
- Boyd SL, Kuhn NC, Patterson JR, Stoll AC, Zimmerman SA, Kolanowski MR, Neubecker JJ, Luk KC, Ramsson ES, Sortwell CE, et al. 2023. Developmental exposure to the Parkinson’s disease-associated organochlorine pesticide dieldrin alters dopamine neurotransmission in α -synuclein pre-formed fibril (PFF)-injected mice. *Toxicol Sci.* 196(1):99–111.

- Brooker SM, Naylor GE, Krainc D. 2024. Cell biology of Parkinson's disease: mechanisms of synaptic, lysosomal, and mitochondrial dysfunction. *Curr Opin Neurobiol.* 85:102841.
- Bu M, Farrer MJ, Khoshbouei H. 2021. Dynamic control of the dopamine transporter in neurotransmission and homeostasis. *NPJ Parkinsons Dis.* 7(1):22.
- Cannon JR, Greenamyre JT. 2013. Gene–environment interactions in Parkinson's disease: specific evidence in humans and mammalian models. *Neurobiol Dis.* 57:38–46.
- Carroll J, Schep A, Sidi J. 2023. ggeasy: easy access to 'ggplot2' commands. The Comprehensive R Archive Network. <https://cloud.r-project.org/package=ggeasy>
- Caudle WM, Guillot TS, Lazo CR, Miller GW. 2012. Industrial toxicants and Parkinson's disease. *Neurotoxicology.* 33(2):178–188.
- Cavalcante RG, Sartor MA. 2017. Annotatr: genomic regions in context. *Bioinformatics.* 33(15):2381–2383.
- Cerri S, Mus L, Blandini F. 2019. Parkinson's disease in women and men: what's the difference? *J Parkinsons Dis.* 9(3):501–515.
- Cicchetti F, Drouin-Ouellet J, Gross RE. 2009. Environmental toxins and Parkinson's disease: what have we learned from pesticide-induced animal models? *Trends Pharmacol Sci.* 30(9):475–483.
- Collier TJ, Kanaan NM, Kordower JH. 2011. Ageing as a primary risk factor for Parkinson's disease: evidence from studies of non-human primates. *Nat Rev Neurosci.* 12(6):359–366.
- Conway JR, Lex A, Gehlenborg N. 2017. UpSetR: an R package for the visualization of intersecting sets and their properties. *Bioinformatics.* 33(18):2938–2940.
- Corrigan FM, Wienburg CL, Shore RF, Daniel SE, Mann D. 2000. Organochlorine insecticides in substantia nigra in Parkinson's disease. *J Toxicol Environ Health A.* 59(4):229–234.
- Cory-Slechta DA, Thiruchelvam M, Richfield EK, Barlow BK, Brooks AI. 2005. Developmental pesticide exposures and the Parkinson's disease phenotype. *Birth Defects Res A Clin Mol Teratol.* 73(3):136–139.
- Dabrowski A, Terauchi A, Strong C, Umemori H. 2015. Distinct sets of FGF receptors sculpt excitatory and inhibitory synaptogenesis. *Development.* 142(10):1818–1830.
- Darling TK, Lamb TJ. 2019. Emerging roles for eph receptors and ephrin ligands in immunity. *Front Immunol.* 10:1473.
- Decressac M, Volakakis N, Björklund A, Perlmann T. 2013. NURR1 in Parkinson disease—from pathogenesis to therapeutic potential. *Nat Rev Neurol.* 9(11):629–636.
- Deidda G, Bozarth IF, Cancedda L. 2014. Modulation of GABAergic transmission in development and neurodevelopmental disorders: investigating physiology and pathology to gain therapeutic perspectives. *Front Cell Neurosci.* 8:119.
- Dluzen DE, McDermott JL. 2000. Gender differences in neurotoxicity of the nigrostriatal dopaminergic system: implications for Parkinson's disease. *J Gend Specif Med.* 3(6):36–42.
- Dorsey ER, Constantinescu R, Thompson JP, Biglan KM, Holloway RG, Kieburtz K, Marshall FJ, Ravina BM, Schifitto G, Siderowf A, et al 2007. Projected number of people with Parkinson disease in the most populous nations, 2005 through 2030. *Neurology.* 68(5):384–386.
- Dorsey ER, Elbaz A, Nichols E, Abd-Allah F, Abdelalim A, Adsuar JC, Ansha MG, Brayne C, Choi JYJ, Collado-Mateo D, et al. 2018a. Global, regional, and national burden of Parkinson's disease, 1996–2016: a systematic analysis for the Global Burden of Disease Study 2016. *Lancet Neurol.* 17(2016):939–953.
- Dorsey ER, Sherer T, Okun MS, Bloem BR. 2018b. The emerging evidence of the Parkinson pandemic. *J Parkinsons Dis.* 8(s1):S3–S8.
- Doucet-Beaupré H, Ang SL, Lévesque M. 2015. Cell fate determination, neuronal maintenance and disease state: the emerging role of transcription factors Lmx1a and Lmx1b. *FEBS Lett.* 589(24 Pt A):3727–3738.
- Ernst A, Böhler L, Hagenston AM, Hoffmann A, Heiland S, Sticht C, Bendzus M, Hecker M, Bading H, Marti HH, et al. 2019. EphB2-dependent signaling promotes neuronal excitotoxicity and inflammation in the acute phase of ischemic stroke. *Acta Neuropathol Commun.* 7(1):15.
- Faulk C, Dolinoy DC. 2011. Timing is everything: the when and how of environmentally induced changes in the epigenome of animals. *Epigenetics.* 6(7):791–797.
- Feng H, Conneely KN, Wu H. 2014. A bayesian hierarchical model to detect differentially methylated loci from single nucleotide resolution sequencing data. *Nucleic Acids Res.* 42(8):e69.
- Fernández-Santiago R, Sharma M. 2022. What have we learned from genome-wide association studies (GWAS) in Parkinson's disease? *Ageing Res Rev.* 79:101648.
- Fleming L, Mann JB, Bean J, Briggles T, Sanchez-Ramos JR. 1994. Parkinson's disease and brain levels of organochlorine pesticides. *Ann Neurol.* 36(1):100–103.
- Fleming SM. 2017. Mechanisms of gene-environment interactions in Parkinson's disease. *Curr Environ Health Rep.* 4(2):192–199.
- Freire C, Koifman S. 2012. Pesticide exposure and Parkinson's disease: epidemiological evidence of association. *Neurotoxicology.* 33(5):947–971.
- Gamit N, Dharmarajan A, Sethi G, Warriar S. 2023. Want of Wnt in Parkinson's disease: could sFRP disrupt interplay between Nurr1 and Wnt signaling? *Biochem Pharmacol.* 212:115566.
- Georgiev D, Hamberg K, Hariz M, Forsgren L, Hariz G. 2017. Gender differences in Parkinson's disease: a clinical perspective. *Acta Neurol Scand.* 136(6):570–584.
- Gezer AO, Kochmanski J, VanOeveren SE, Cole-Strauss A, Kemp CJ, Patterson JR, Miller KM, Kuhn NC, Herman DE, McIntire A, et al. 2020. Developmental exposure to the organochlorine pesticide dieldrin causes male-specific exacerbation of α -synuclein-preformed fibril-induced toxicity and motor deficits. *Neurobiol Dis.* 141:104947.
- Gillies GE, Pienaar IS, Vohra S, Qamhawi Z. 2014. Sex differences in Parkinson's disease. *Front Neuroendocrinol.* 35(3):370–384.
- Gionco JT, Bernstein AI. 2024. Emerging role of environmental epitranscriptomics and RNA modifications in Parkinson's disease. *J Parkinsons Dis.* 14(4):643–656.
- Goldman SM. 2014. Environmental toxins and Parkinson's disease. *Annu Rev Pharmacol Toxicol.* 54:141–164.
- Goldman SM, Musgrove RE, Jewell SA, Monte DAD. 2017. Chapter three—pesticides and Parkinson's disease: current experimental and epidemiological evidence. *Adv Neurotoxicol.* 1:83–117.
- Haaxma CA, Bloem BR, Borm GF, Oyen WJG, Leenders KL, Eshuis S, Booij J, Dluzen DE, Horstink MWIM. 2007. Gender differences in Parkinson's disease. *J Neurol Neurosurg Psychiatry.* 78(8):819–824.
- Hatcher JM, Richardson JR, Guillot TS, McCormack AL, Monte DAD, Jones DP, Pennell KD, Miller GW. 2007. Dieldrin exposure induces oxidative damage in the mouse nigrostriatal dopamine system. *Exp Neurol.* 204(2):619–630.
- Heindel JJ, Vandenberg LN. 2015. Developmental origins of health and disease: a paradigm for understanding disease cause and prevention. *Curr Opin Pediatr.* 27(2):248–253.
- Hilz EN, Gore AC. 2022. Sex-specific effects of endocrine-disrupting chemicals on brain monoamines and cognitive behavior. *Endocrinology.* 163(10):bqac128.

- Hochberg Z, Feil R, Constancia M, Fraga M, Junien C, Carel J, Boileau P, Le Bouc Y, Deal CL, Lillycrop K, et al. 2011. Child health, developmental plasticity, and epigenetic programming. *Endocr Rev.* 32(2):159–224.
- Hong J, Kim HY, Kim DG, Seo J, Kim KJ. 2004. Rapid determination of chlorinated pesticides in fish by freezing-lipid filtration, solid-phase extraction and gas chromatography-mass spectrometry. *J Chromatogr A.* 1038(1-2):27–35.
- Jakaria M, Haque ME, Cho DY, Azam S, Kim IS, Choi DK. 2019. Molecular insights into NR4A2(Nurr1): an emerging target for neuroprotective therapy against neuroinflammation and neuronal cell death. *Mol Neurobiol.* 56(8):5799–5814.
- Jorgenson JL. 2001. Aldrin and dieldrin: a review of research on their production, environmental deposition and fate, bioaccumulation, toxicology, and epidemiology in the United States. *Environ Health Perspect.* 109(Suppl 1):113–139.
- Jurado-Coronel JC, Cabezas R, Rodríguez MFÁ, Echeverría V, García-Segura LM, Barreto GE. 2018. Sex differences in Parkinson's disease: features on clinical symptoms, treatment outcome, sexual hormones and genetics. *Front Neuroendocrinol.* 50:18–30.
- Kaizuka T, Takumi T. 2024. Alteration of synaptic protein composition during developmental synapse maturation. *Eur J Neurosci.* 59(11):2894–2914.
- Kania A, Klein R. 2016. Mechanisms of ephrin-Eph signalling in development, physiology and disease. *Nat Rev Mol Cell Biol.* 17(4):240–256.
- Kassambara A. 2023. ggpubr: 'ggplot2' based publication ready plots. The Comprehensive R Archive Network. <https://cran.r-project.org/web/packages/ggpubr/index.html>
- Keller MF, Saad M, Bras J, Bettella F, Nicolaou N, Simón-Sánchez J, Mittag F, Büchel F, Sharma M, Gibbs JR, et al.; Wellcome Trust Case Control Consortium 2 (WTCCC2). 2012. Using genome-wide complex trait analysis to quantify 'missing heritability' in Parkinson's disease. *Hum Mol Genet.* 21(22):4996–5009.
- Klimaschewski L, Claus P. 2021. Fibroblast growth factor signalling in the diseased nervous system. *Mol Neurobiol.* 58(8):3884–3902.
- Kochmanski J, Bernstein AI. 2020. The impact of environmental factors on 5-hydroxymethylcytosine in the brain. *Curr Environ Health Rep.* 7(2):109–120.
- Kochmanski J, Montrose L, Goodrich JM, Dolinoy DC. 2017. Environmental deflection: the impact of toxicant exposures on the aging epigenome. *Toxicol Sci.* 156(2):325–335.
- Kochmanski J, VanOeveren SE, Patterson JR, Bernstein AI. 2019. Developmental dieldrin exposure alters DNA methylation at genes related to dopaminergic neuron development and Parkinson's disease in mouse midbrain. *Toxicol Sci.* 169(2):593–607.
- Kozomara A, Birgaoanu M, Griffiths-Jones S. 2019. miRBase: from microRNA sequences to function. *Nucleic Acids Res.* 47(D1):D155–D162.
- Kraft AD, Aschner M, Cory-Slechta DA, Bilbo SD, Caudle WM, Makris SL. 2016. Unmasking silent neurotoxicity following developmental exposure to environmental toxicants. *Neurotoxicol Teratol.* 55:38–44.
- Krueger F. 2017. Trim Galore! Version 4.5. Babraham Institute. https://www.bioinformatics.babraham.ac.uk/projects/trim_galore/
- Krueger F, Andrews SR. 2011. Bismark: a flexible aligner and methylation caller for bisulfite-seq applications. *Bioinformatics.* 27(11):1571–1572.
- Kundaje A, Collins PJ, Davis CA, Khatun J, Lajoie BR, Landt SG, Safi A, Altshuler RC, Cheng C, Greven M, et al.; ENCODE Project Consortium. 2012. An integrated encyclopedia of DNA elements in the human genome. *Nature.* 489(7414):57–74.
- Larsson J. 2024. eulerr: area-proportional Euler and Venn diagrams with ellipses. The Comprehensive R Archive Network. <https://cran.r-project.org/web/packages/eulerr/index.html>
- Li D, Purushotham D, Harrison JK, Hsu S, Zhuo X, Fan C, Liu S, Xu V, Chen S, Xu J, et al. 2022. WashU epigenome browser update 2022. *Nucleic Acids Res.* 50(W1):W774–W781.
- Lill CM. 2016. Genetics of Parkinson's disease. *Mol Cell Probes.* 30(6):386–396.
- Lim C, Hanspers K, Sklar S, Willighagen E, Evelo C, Summer-Kutmon M, Weitz E. 2024. Dopaminergic neurogenesis (WP1498)—Mus musculus. WikiPathways. <https://www.wikipathways.org/pathways/WP1498.html>
- Liu X, Hua F, Yang D, Lin Y, Zhang L, Ying J, Sheng H, Wang X. 2022. Roles of neuroligins in central nervous system development: focus on glial neuroligins and neuron neuroligins. *J Transl Med.* 20(1):418.
- Luderman KD, Chen R, Ferris MJ, Jones SR, Gnegy ME. 2015. Protein kinase C beta regulates the D₂-like dopamine autoreceptor. *Neuropharmacology.* 89:335–341.
- Luo Y, Hitz BC, Gabdank I, Hilton JA, Kagda MS, Lam B, Myers Z, Sud P, Jou J, Lin K, et al. 2020. New developments on the encyclopedia of DNA elements (ENCODE) data portal. *Nucleic Acids Res.* 48(D1):D882–D889.
- Marras C, Beck JC, Bower JH, Roberts E, Ritz B, Ross GW, Abbott RD, Savica R, Van Den Eeden SK, Willis AW, et al.; Parkinson's Foundation P4 Group. 2018. Prevalence of Parkinson's disease across North America. *NPJ Parkinsons Dis.* 4:21.
- McCabe C, Anderson OS, Montrose L, Neier K, Dolinoy DC. 2017. Sexually dimorphic effects of early-life exposures to endocrine disruptors: sex-specific epigenetic reprogramming as a potential mechanism. *Curr Environ Health Rep.* 4(4):426–438.
- Moretto A, Colosio C. 2011. Biochemical and toxicological evidence of neurological effects of pesticides: the example of Parkinson's disease. *Neurotoxicology.* 32(4):383–391.
- Narahashi T. 1996. Neuronal ion channels as the target sites of insecticides. *Pharmacol Toxicol.* 79(1):1–14.
- Narahashi T, Carter DB, Frey J, Ginsburg K, Hamilton BJ, Nagata K, Roy ML, Song JH, Tatebayashi H. 1995. Sodium channels and GABAA receptor-channel complex as targets of environmental toxicants. *Toxicol Lett.* 82–83:239–245.
- Oliveira MAP, Balling R, Smidt MP, Fleming RMT. 2017. Embryonic development of selectively vulnerable neurons in Parkinson's disease. *NPJ Parkinsons Dis.* 3:21.
- Peters TJ, Buckley MJ, Statham AL, Pidsley R, Samaras K, V Lord R, Clark SJ, Molloy PL. 2015. De novo identification of differentially methylated regions in the human genome. *Epigenetics Chromatin.* 8:6.
- Pozniak PD, White MK, Khalili K. 2014. TNF- α /NF- κ B signaling in the CNS: possible connection to EPHB2. *J Neuroimmune Pharmacol.* 9(2):133–141.
- Quinlan AR. 2014. BEDTools: the Swiss-Army tool for genome feature analysis. *Curr Protoc Bioinformatics.* 47:11.12.1–11.12.34.
- Quinlan AR, Hall IM. 2010. BEDTools: a flexible suite of utilities for comparing genomic features. *Bioinformatics.* 26(6):841–842.
- Rasmussen AH, Rasmussen HB, Silaharoglu A. 2017. The DLGAP family: neuronal expression, function and role in brain disorders. *Mol Brain.* 10(1):43.
- Richardson JR, Caudle WM, Wang M, Dean ED, Pennell KD, Miller GW. 2006. Developmental exposure to the pesticide dieldrin alters the dopamine system and increases neurotoxicity in an animal model of Parkinson's disease. *FASEB J.* 20(10):1695–1697.

- Schaffner SL, Kobor MS. 2022. DNA methylation as a mediator of genetic and environmental influences on Parkinson's disease susceptibility: impacts of alpha-synuclein, physical activity, and pesticide exposure on the epigenome. *Front Genet.* 13:971298.
- Scheltinga AFTV, Bakker SC, Kahn RS, Kas MJH. 2013. Fibroblast growth factors in neurodevelopment and psychopathology. *Neuroscientist.* 19(5):479–494.
- Sen A, Hongpaisan J, Wang D, Nelson TJ, Alkon DL. 2016. Protein kinase C ϵ (PKC ϵ) promotes synaptogenesis through membrane accumulation of the postsynaptic density protein PSD-95. *J Biol Chem.* 291(32):16462–16476.
- Sloniowski S, Ethell IM. 2012. Looking forward to EphB signaling in synapses. *Semin Cell Dev Biol.* 23(1):75–82.
- Smoot ME, Ono K, Ruschinski J, Wang P, Ideker T. 2011. Cytoscape 2.8: new features for data integration and network visualization. *Bioinformatics.* 27(3):431–432.
- Soukup S, Vanhauwaert R, Verstreken P. 2018. Parkinson's disease: convergence on synaptic homeostasis. *EMBO J.* 37(18):e98960.
- Stevens HE, Scuderi S, Collica SC, Tomasi S, Horvath TL, Vaccarino FM. 2023. Neonatal loss of FGFR2 in astroglial cells affects locomotion, sociability, working memory, and glia-neuron interactions in mice. *Transl Psychiatry.* 13(1):89.
- Stevens HE, Smith KM, Rash BG, Vaccarino FM. 2010. Neural stem cell regulation, fibroblast growth factors, and the developmental origins of neuropsychiatric disorders. *Front Neurosci.* 4:59.
- Südhof TC. 2023. Cerebellin-neurexin complexes instructing synapse properties. *Curr Opin Neurobiol.* 81:102727.
- Sulzer D. 2007. Multiple hit hypotheses for dopamine neuron loss in Parkinson's disease. *Trends Neurosci.* 30(5):244–250.
- Svoboda LK, Ishikawa T, Dolinoy DC. 2022a. Developmental toxicant exposures and sex-specific effects on epigenetic programming and cardiovascular health across generations. *Environ Epigenet.* 8(1):dvac017.
- Svoboda LK, Perera BPU, Morgan RK, Polemi KM, Pan J, Dolinoy DC. 2022b. Toxicopigenetics and environmental health: challenges and opportunities. *Chem Res Toxicol.* 35(8):1293–1311.
- Szklarczyk D, Franceschini A, Wyder S, Forslund K, Heller D, Huerta-Cepas J, Simonovic M, Roth A, Santos A, Tsafou KP, et al. 2015. STRING v10: protein–protein interaction networks, integrated over the tree of life. *Nucleic Acids Res.* 43(Database issue):D447–D452.
- Szklarczyk D, Morris JH, Cook H, Kuhn M, Wyder S, Simonovic M, Santos A, Doncheva NT, Roth A, Bork P, et al. 2017. The STRING database in 2017: quality-controlled protein–protein association networks, made broadly accessible. *Nucleic Acids Res.* 45(D1):D362–D368.
- Trinh J, Farrer M. 2013. Advances in the genetics of Parkinson disease. *Nat Rev Neurol.* 9(8):445–454.
- Tsalenchuk M, Gentleman SM, Marzi SJ. 2023. Linking environmental risk factors with epigenetic mechanisms in Parkinson's disease. *NPJ Parkinsons Dis.* 9(1):123.
- Tunster SJ. 2017. Genetic sex determination of mice by simplex PCR. *Biol Sex Differ.* 8(1):31.
- U.S. Environmental Protection Agency. 1994. Semivolatile organic compounds in the general U.S. population: NHATS FY86 results—Volume I. Washington (DC).
- US Environmental Protection Agency. 2014. Method 3620C florisil cleanup, update V. Washington (DC).
- Van Den Eeden SK, Tanner CM, Bernstein AL, Fross RD, Leimpeter A, Bloch DA, Nelson LM. 2003. Incidence of Parkinson's disease: variation by age, gender, and race/ethnicity. *Am J Epidemiol.* 157(11):1015–1022.
- Vu H, Ernst J. 2023. Universal chromatin state annotation of the mouse genome. *Genome Biol.* 24(1):153.
- WHO-IPCS (World Health Organization—International Programme on Chemical Safety). 1989. Aldrin and dieldrin. *Environmental health criteria* 91. Geneva.
- Willis AW, Evanoff BA, Lian M, Criswell SR, Racette BA. 2010. Geographic and ethnic variation in Parkinson disease: a population-based study of US medicare beneficiaries. *Neuroepidemiology.* 34(3):143–151.
- Willis AW, Roberts E, Beck JC, Fiske B, Ross W, Savica R, Van Den Eeden SK, Tanner CM, Marras C; Parkinson's Foundation P4 Group. 2022. Incidence of Parkinson disease in North America. *NPJ Parkinsons Dis.* 8(1):170.
- Yang J, Wei H, Chen P, Wu G. 2018. Roles of eph/ephrin bidirectional signaling in central nervous system injury and recovery (review). *Exp Ther Med.* 15(3):2219–2227.
- Yang W, Hamilton JL, Kopil C, Beck JC, Tanner CM, Albin RL, Ray Dorsey E, Dahodwala N, Cintina I, Hogan P, et al. 2020. Current and projected future economic burden of Parkinson's disease in the U.S. *NPJ Parkinsons Dis.* 6:15.
- Yao Z, van Velthoven CTJ, Kunst M, Zhang M, McMillen D, Lee C, Jung W, Goldy J, Abdelhak A, Aitken M, et al. 2023. A high-resolution transcriptomic and spatial atlas of cell types in the whole mouse brain. *Nature.* 624(7991):317–332.